CHAPTER 4. SENSITIVITY ANALYSIS AND TESTING

L. Zhang, W. R. Dawes, T. J. Hatton,
and P. Dyce

4.1 Introduction

WAVES is a complex process-based model and it attempts to represent the key processes with a fair degree of physical fidelity. As a result, a sensitivity analysis of all inputs over their potential range and complexity is not feasible. Thus we take a more pragmatic and constrained approach to model sensitivity analysis in this study. We are aided in setting constraints by the physical nature of the parameterisation. Further, with an understanding of model structure and the underlying physics and physiology, it is possible to identify *a priori* a set of key parameters to which the model is most sensitive. This section presents such an analysis and discussion of the behaviour of the WAVES model to perturbation of selected set of input parameters.

4.2 Site Description and Data Collection

The sensitivity analysis was conducted using data from an experimental area in a 109-ha mixed cropping catchment named ‘Tambea’, at Wagga Wagga, N.S.W. (35°10' S and 147°18' E). In the 1992 and 1993 seasons, the crops sown were canola, oats and wheat. The soils of the experimental area formed on granite parent material. The dominant soil type, Red Earth (haplic eutrophic red kandasol), comprises weakly structured clay loam to light clay, red in colour and free of stone and coarse sand. The upper slopes and low rounded crests have *in situ* red podzolics (haplic mesotrophic red chromosol) which grade into weathered granite at less than 1 m. On the main drainage line, the soils are formed of colluvium overlying a clay that appears to have developed *in situ* on the granite.

Various data relating to climate, soil water content, and plant growth were collected over two winter growing seasons from June 1992 to January 1994, separated by fallow. The growing season and fallow period from June 1992 to June 1993 was used to calibrate the free parameters. The subsequent growing season until January 1994 was used as a validation period, where no parameters were changed, only water balance and plant growth estimates examined.

One year is a short time to calibrate a complex physical model. However, at this latitude there is a large variation in the climatic inputs over a year. Given that the annual crops grew in winter with an abundance of resources, we needed only to fit four critical plant growth parameters. During the summer months when the area was fallow, we could fit the soil moisture profiles with a single parameter without the need to fit plant growth in parallel. The results presented in Section 4 will show that the calibration obtained from the first year produced good results in the second year.

Soil hydraulic properties

Soil hydraulic conductivity was estimated at various depths using a well permeameter, or Gleuph type infiltrometer, at 12 sites in the catchment that included the three main soil groups. Total soil depth was estimated from the depth at which conductivity reduced to near zero. Saturated and air-dry volumetric water contents were estimated from the range of water contents reported from the soil moisture monitoring, and from soil descriptions reported in Forrest *et al.* (1985). Values of the capillary length scale, l_C, and the soil structure parameter, C, were estimated from moisture characteristics reported by Forrest *et al.* (1985) and soil texture and structure descriptions from Fogarty (1992). Hydraulic conductivity was adjusted downwards during calibration to match observed soil moisture profiles.

Climatic data

Climatic data collected on site at Tambea was measured with an automatic weather station. Wet and dry bulb temperatures were measured using temperature sensors with a standard muslin and wick changed fortnightly. A Rimik tipping bucket rain gauge recorded rainfall amount and intensity. A three cup anemometer with 64mm diameter cups mounted 2m above ground level was used to record windrun. Radiation sensors with a spectrum response < –3dB from 500 to 1000 nm were used to record total global radiation and reflected solar radiation. Additional climatic data was collected at ‘Shanagh’, approximately 1 km northeast of ‘Tambea’, with a similar range of sensors.

Soil moisture measurement

During the period 1992 to 1993, soil moisture contents were measured fortnightly at 11 sites across the area using a modified Tektronix Time Domain Reflectometry (PYELAB TDR SYSTEM) and CSIRO Software. Probes were inserted horizontally at up to five depths below the surface; due to considerations of the experimental budget, placing more probes at regular depths was not done. Individual calibrated probes were read manually in the field every 2 to 4 weeks, and stored traces were reanalyzed and compared with volumetric soil moisture estimates to check the accuracy of the measurements.

Leaf area index

The leaf area index (LAI) was measured on monthly intervals throughout the growing season. In each of the paddocks at Tambea, three randomly placed 1-m^2 quadrats were clipped to ground level. The one-sided green leaf area was measured using an electronic planimeter. The leaf areas for each of the three quadrats was averaged to give a single value for each paddock. Frequent checking, and if necessary, fine adjustment of the planimeter was carried out using known standards to maintain accuracy to at least 5%.

Total evaporation

Poss *et al*. (1995) made measurements of evaporation using lysimeters in an adjacent catchment. Data from June 1992 to December 1993 was collected at 1- to 4-week intervals; a total of 23 data points. The total evaporation modelled by WAVES was aggregated over the same periods, averaged for the number of days in each measurement period and compared directly.

Streamflow measurement

Total catchment runoff was measured using a modified V-notch weir. Flow heights were measured at two stilling wells using 'Wesdata' capacitance probes and 390 series data loggers. A low flow rate calibration curve was derived by measurements taken using a 'Hydrological Services' OSS PC1 current meter. Due to the extremely small amount of runoff and stream flow, only low flows occurred, and were recorded, during the simulated period.

4.3 Method

The model was first calibrated for Site D, over a period of 15 months (27 April 1992 to June 1994). Model inputs were adjusted to achieve the best agreement between predicted and measured LAI for the wheat crop. The parameters adjusted were: plant maximum assimilation of carbon; the IRM weightings of water and nutrients relative to light, and the plant respiration coefficients. We recognised that resultant parameter set is not unique but it does present a plausible model of wheat growth for the Tambea catchment. This calibrated base set of parameters was used to test the sensitivity WAVES in this analysis. These parameters are essentially those used in part by Dawes *et al*. (1997) in simulations of this catchment.

We recognise that with the use of this simulation alone it isn't possible to produce a completely comprehensive analysis of all variables, especially for other vegetation types and soils. The sensitivity analysis was conducted in a standard manner in which the model was run with the value of single parameter altered by plus and minus 10%, holding all other variables constant. The climatic inputs to the model were constant for all iterations.

The soil parameters were handled as a special case. As it often the case, the soil as described for Site D was modelled as a set of layers with distinct hydraulic properties. In those simulations testing the sensitivity of any one soil parameter, the values of that parameter were altered by the same amount in each layer throughout the profile. The rationale behind this scheme is purely pragmatic; model sensitivity to a change in a soil hydraulic parameter in any single, arbitrary layer will be chaotic with respect to the position this layer holds in relation to the rest of the profile.

4.4 Results and Discussion

The selected parameters were compared with a set of model outputs. These outputs were used as indicators of performance and are commonly used in comparing modelling scenarios. The outputs are: evaporation from vegetation (transpiration, E_v) and soil (E_s) to indicate changes in energy flux; deep drainage (DD) to indicate effect on the soil water balance; and maximum leaf area index for the growing season (LAI_{max}) to indicate effects on plant growth. The results are summarised in Table 4.1.

The calculated transpiration is sensitive to the maximum assimilation rate of carbon (A_{max}), the slope of the stomatal conductance model (g_1), canopy albedo (α_v), and the soil shape parameter (C). The actual assimilation rate of carbon is closely related to its maximum value; equation (21) shows that the canopy resistance is inversely proportional to the actual assimilation rate. As a result, changes associated with A_{max} affects canopy transpiration; g_1 influences transpiration in a similar way. The parameters A_{max} and g_1 are related to canopy resistance and the discussions are valid for canopies with similar aerodynamic characteristics (*e.g.* roughness length). Changes in canopy resistance caused by these parameters may have different degrees of effects on transpiration depending upon the roughness length of the canopy. The predicted value of transpiration is sensitive to the canopy resistance when the aerodynamic resistance is relatively small (*e.g.* tall crops and forests). At large values of the aerodynamic resistance (*e.g.* short crops and grass), and especially under non-water limited conditions such as were experienced in the two winter growing seasons, the transpiration is much less sensitive to the canopy resistance, and the partitioning of the available energy into sensible and latent heat fluxes is significantly controlled by the aerodynamic resistance. Increased α_v reduces the available energy reaching the canopy surface, hence decreases the transpiration. The shape parameter C, which is related to soil structure, affects transpiration significantly because of its effect on plant available water at a given potential. The next most sensitive parameters are leaf area index and the weightings for water and nutrients, which have reduced effects on canopy transpiration because of the nonlinearity of the relationships between the canopy resistance and these parameters.

Table 4.1. Summary of sensitivity analysis performed on site D for growing season 1992–93. E_v, E_s refer to transpiration from vegetation and evaporation from soil in mm, *Q* is the total drainage in mm, LAI_{max} is the maximum leaf area index. The columns labelled '%' refer to percentage changes from 'control' values. LBC refers to 'lower boundary condition' defined as fraction of saturated hydraulic conductivity. Other symbols are defined in Table 2.1.

Parameter	Change	E_v	$\%E_v$	E_s	$\%E_s$	Q	%Q	LAI_{max}	$\%LAI_{max}$
				Standard					
		196.3	----	406.0	----	30.6	----	3.2	----
α_S	+	198.4	+1.1	393.6	–3.0	30.8	+0.7	3.2	0.0
	–	193.8	–1.3	418.2	+3.0	30.3	–0.8	3.2	0.0
α_V	+	178.3	–9.2	418.9	+3.2	30.7	+0.3	2.9	–9.6
	–	210.0	+7.0	396.4	–2.3	30.5	–0.3	3.5	+9.2
A_{max}	+	224.2	+14.2	378.2	–6.9	30.4	–0.5	4.2	+29.4
	–	159.7	–18.6	439.1	+8.1	30.7	+0.4	2.4	–24.3
LAI	+	190.1	+5.8	423.7	–2.4	30.5	–0.5	3.5	----
	–	167.2	–7.0	445.2	+2.6	30.9	+0.4	2.9	----
K_e	+	196.7	+0.2	402.8	–0.8	30.6	0.0	3.1	–2.9
	–	194.9	–0.7	410.1	+1.0	30.6	0.0	3.3	+3.2
g_1	+	230.2	+17.3	402.7	–0.8	30.5	–0.2	3.2	0.0
	–	188.1	–4.2	409.8	+0.9	30.6	0.0	3.2	0.0
χ_H	+	206.4	+5.1	396.1	–2.4	30.5	–0.5	3.5	+9.9
	–	184.8	–5.8	416.9	+2.6	30.6	0.0	2.9	–9.6
χ_N	+	188.7	–3.8	413.2	+1.8	30.6	0.0	2.9	–6.2
	–	203.9	+3.8	398.6	–1.8	30.5	–0.5	3.4	+7.1
F_l	+	190.5	–3.0	411.9	+1.5	30.6	0.0	3.2	0.0
	–	202.9	+3.4	399.1	–1.7	30.6	0.0	3.2	0.0
LBC	+	196.3	0.0	405.9	0.0	33.4	+9.3	3.2	0.0
	–	196.3	0.0	405.9	0.0	27.7	–9.4	3.2	0.0
K_S	+	196.3	0.0	404.7	–0.3	34.2	+11.7	3.2	0.0
	–	196.2	0.0	407.4	+0.4	26.9	–11.7	3.2	0.0
θ_S	+	199.1	+1.5	417.1	+2.7	29.8	–2.5	3.2	0.0
	–	192.5	–1.9	394.8	–2.7	31.3	+2.4	3.2	0.0
θ_d	+	197.1	+0.4	401.8	–1.0	30.7	+0.3	3.2	0.0
	–	197.4	+0.5	410.1	+0.7	30.5	–0.5	3.2	0.0
λ_c	+	197.4	+0.5	408.7	–0.7	32.0	+4.7	3.2	0.0
	–	194.9	–0.7	403.3	+2.2	28.5	–6.8	3.2	0.0
C	+	178.2	–9.2	415.2	+2.2	29.5	–3.6	3.2	0.0
	–	196.1	–0.1	414.2	+2.0	31.7	+3.6	3.2	0.0

The predicted soil evaporation was relatively sensitive to A_{max}, which affects the soil evaporation indirectly through its effects on canopy transpiration and canopy development (*i.e.* soil shading). The soil hydraulic properties have little influence on the cumulative soil evaporation and this may have the implication that the uncertainties associated with the soil properties will not cause large errors in predicted soil evaporation from TOPOG_IRM. However, other factors such as the formulation of soil surface resistance (*e.g.* equation 2.56) may play a significant role in controlling the soil evaporation.

The total drainage was affected significantly by the lower boundary conditions and the saturated hydraulic conductivity. In WAVES, the lower boundary conditions are defined as a fraction of the saturated hydraulic conductivity ranging from free drainage, where the fraction is one, to no drainage, where the fraction is zero. The lower boundary conditions determine the amount of water potentially drained from the bottom of the soil layer. The results in Table 4.1 showed that a 10% change in either the lower boundary conditions or the saturated hydraulic conductivity could lead to an equivalent change in the total drainage. When the model is applied to study the effects of land-use management on groundwater recharge, these two parameters become critical.

Because of the nonlinear dependence of leaf area index and A_{max}, changes of 10% in the maximum assimilation rate produced changes in the maximum leaf area index of about 25%. The maximum leaf area index was also sensitive to α_v, and the weightings of water and nutrients.

4.5 Summary

The plant growth model in WAVES is particularly sensitive to the maximum assimilation rate, and under certain conditions, to the IRM weighting factors. The potential feedback, direct and indirect, on the surface water balance are significant. Of the soil parameters, conductivity appears to most drastically affect deep drainage. Although not demonstrated in this series of simulation, the other hydraulic parameters do have significant effect on the shape of the soil moisture profile. The conductivity of the lower boundary of the numerical soil water redistribution model was of paramount importance to the magnitude of deep drainage; the extreme sensitivity to this condition has serious implications to any soil water balance model predicated on a continuity equation for moisture redistribution.

4.6 Testing energy balance components

The following experiment was designed to test the energy balance component of WAVES under controlled conditions. The meteorological inputs have the following characteristics:

$R_{sd} = 312\ W/m^2$ (shortwave downward radiation)

$T_a = 20\ ^{\circ}C$ (average air temperature)

$e_a = 12.0\ hPa$ (average vapour pressure)

$K_s = 0.60$ (light extinction coefficient)

$L_1 = 3.0$ (leaf area index)

$\alpha_1 = 0.22$ (canopy albedo)

$\alpha_s = 0.22$ (surface albedo)

We assumed one vegetation layer plus one soil layer. The soil was loam with the total depth of 100 cm. For simplicity, precipitation, runoff and drainage were assumed to be zero and the simulation started with saturated soil moisture content throughout the soil profile. Therefore, the maximum annual evapotranspiration should equal to the total available water in the soil layer. In what follows, we will first calculate radiation budget and its partitioning between the vegetation canopy and the soil surface. Then we will show the simulated energy balance from WAVES for the vegetation and soil layers. This will provide a diagnostic check on the energy balance component of the model.

The radiation budget is calculated as:

$$e_a = 1.24(12/(273.15+20))^{1/7} = 0.79$$

$$R_{ld} = 0.79 * 5.6697 * 10^{-8} * (273.15 + 20.0)^4 = 330.0\,W/m^2$$

$$R_{lu} = 1.0 * 5.6697 * 10^{-8} * (273.15 + 20.0)^4 = 418.0\,W/m^2$$

For the vegetation layer

$$R_{sv1}\downarrow = 312(1 - exp(-0.60 * 3.0)) = 260.0 W/m^2$$

$$R_{sv1}\uparrow = 312 * 0.22(1 - exp(-0.60 * 3.0)) = 57.2 W/m^2$$

$$R_{lv1}\downarrow = 330.0(1 - exp(-0.66 * 3.0)) = 275.0 W/m^2$$

$$R_{lv1}\uparrow = 418(1 - exp(-0.6 * 3.0)) = 349.0 W/m^2$$

The net radiation for the vegetation layer is

$$R_{nv1} = 260 - 57 + 275 - 349 = 129.0\ W/m^2$$

For the soil layer

$$R_{sg}\downarrow = 312\,exp(-0.6*3.0) = 52\ W/m^2$$

$$R_{sg}\uparrow = 312*0.22\,exp(-0.6*3.0) = 11.0\ W/m^2$$

$$R_{lg}\downarrow = 330\,exp(-0.6*3.0) = 54.0\ W/m^2$$

$$R_{lg}\uparrow = 418\,exp(-0.6*3.0) = 69.0\ W/m^2$$

The net radiation for the soil layer is

$$R_{ng} = 52 - 1.0 + 54.0 - 69.0 = 26.0\ W/m^2$$

Therefore, the total net radiation received by the system (vegetation + soil) is

$$R_n = R_{nvl} + R_{ng} = 129.0 + 26.0 = 155\ W/m^2$$

The simulated net radiation from WAVES are 129.0 and 26.0 W/m^2 for the vegetation and soil layers respectively. It is clear that the radiation and its partitioning in WAVES is as expected. The energy balance components during the period of simulation are shown in Fig. 4.1. The total evapotranspiration was 315.9 mm, which is almost identical to the available water in the soil layer (*i.e*. 316.0 mm). Although this is not a complete test for the energy balance, it provided a diagnostic check on the energy balance and indicated that energy is neither created nor destroyed in the system.

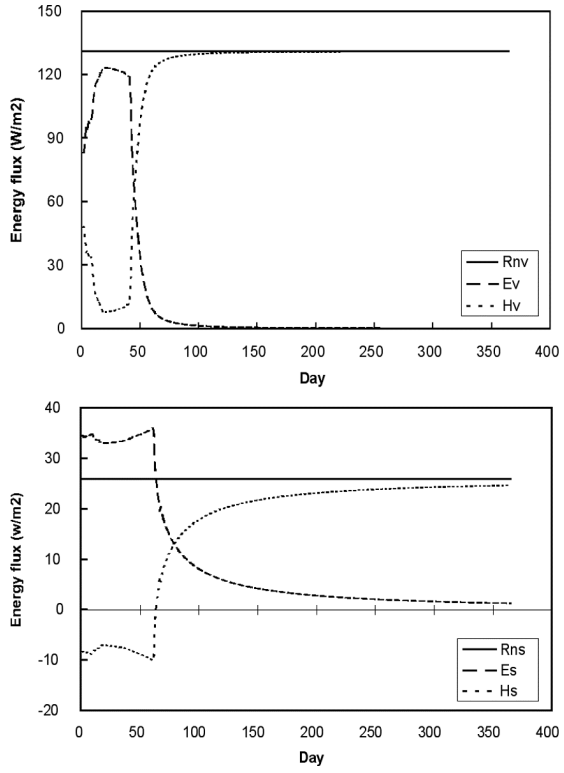

Fig. 4.1. Time course of net radiation, evapotranspiration, and sensible heat flux simulated by WAVES. R_n, E, H represent net radiation, evaporation, and sensible heat flux, respectively. Subscripts v and s represent vegetation canopy and soil.

4.7 Testing water balance component

A summary table is reported at the end of each simulation to ensure a perfect mass balance for water. In most cases, the model will achieve good mass balance. When errors occur in mass balance, users will be notified and should check their input files for possible errors. Following table is an example of mass balance for water. The results are obtained from a simulation using data from Griffith, NSW. It is clear that model achieved a perfect mass balance for water.

Table 4.2. Check for Mass Balance of Water

Initial Storage (mm)	505.50
Final Storage (mm)	407.81
Change in Storage (mm)	–97.69
Total Gross Rainfall (mm)	1500.00
Total Overstorey Interception (mm)	193.06
Total Understorey Interception (mm)	0.00
Total Net Rainfall (mm)	1306.94
Total Evaporation from soil (mm)	454.08
Total Overstorey Transpiration (mm)	986.20
Total Understorey Transpiration (mm)	0.00
Total Evapotranspiration (mm)	1440.29
Total Lateral Fluxes (mm)	0.00
Total Overland Flow (mm)	125.46
Total Deep Drainage (mm)	0.00
Total Flood Extra (mm)	0.00
Total Groundwater Extra (mm)	161.13
Total Groundwater Changes (mm)	0.00
Mass Balance Error (mm)	0.000000

4.8 Testing solute balance component

Similar to the mass balance for water, a summary table for solute is also reported at the end of each simulation when involving solute transport. The following summary table was obtained from WAVES simulation for lucerne grown in a lysimeter in Griffith, NSW. A nonsaline watertable (EC 0.1 dS m^{-1}) at 60 cm below the soil surface was established before sowing and was later dropped to 100 cm using the Mariotte tanks. When the lucerne fully established, a saline watertable was introduced (EC 16 dS m^{-1}) and maintained at 100 cm depth until the end of the experiment. It is clear that most of the solute came from the saline watertable as a result of upward flux of water and transpiration. Rain and irrigation water contributed a little to the total solute in the soil profile. It is obvious that WAVES obtained a perfect mass balance for solute.

Table 4.3. Check for Mass Balance of Solute

Initial Solute Mass (kg)	0.00
Final Solute Mass (kg)	3.10
Solute from Surface (kg)	0.08
Solute from Basement (kg)	3.02
Solute from Lateral Flows (kg)	0.00
Mass Balance Error (kg)	0.000000

4.9 Guaranteeing Numerical Convergence and Stability of Finite Difference Solutions of Richards' Equation

D. L. Short*, W. R. Dawes
CSIRO Land and Water, Canberra, Australian Capital Territory

I. White
Centre for Resource and Environmental Studies, ANU, Canberra, Australian Capital Territory

Abstract

Two distinctive features of the soil hydraulic model of *Broadbridge and White* (1988) permit guaranteeing *a priori* the numerical performance of finite difference solutions of Richards' soil-water flow equation, for a wide range of nonlinearity of soil hydraulic properties. Firstly, soil-water diffusivity remains (realistically) finite as soil becomes either very dry or 'saturated'. Thus solutions of the differential and finite difference equations remain determinate under all conditions. Secondly, hydraulic functions may be scaled across all soils described by the model, and finite difference solutions scaled in terms of space-step, time-step and transformed rainfall rate. The critically difficult case of constant-rate infiltration into semi-infinite dry soil permits numerical performance to be investigated comprehensively, using only a three-dimensional parameter space. A particularly efficient numerical scheme is identified. Scaled solutions for cases of coarse fixed space-time mesh correspond closely to analytical solutions, without propagation of short-time errors, for both semi-infinite and finite depth soils. Criteria are developed for guaranteed numerical convergence and stability, for Crank–Nicolson and backward difference schemes. Scaling and determinacy are proposed for comprehensively testing alternative numerical schemes.

---

* Now an independent scientific consultant.

4.9.1 Introduction

Because of advances in numerical techniques, numerical solutions of the soil-water flow equation of *Richards* (1931) are now available for a wide range of practical situations (e.g. *Brutsaert*, 1971; *Ross*, 1990). However, general use of numerical solutions is restricted by our inability to robustly predict numerical convergence and stability.

There appear to be no reports of making such predictions *a priori* for arbitrary space and time steps and rainfall rates, for a wide range of soil hydraulic properties. Sometimes it is stated that convergence and stability can be 'guaranteed' (e.g. *Celia et al.*, 1990; *Li*, 1993). However, these guarantees are not *a priori* in that time-steps are controlled dynamically, and space steps appear to be based on knowledge of a limited range of soil hydraulic properties and boundary conditions.

For linear convective-diffusive equations (CDE), criteria for numerical stability are readily derived (e.g. *Noye*, 1990) by scaling four parameters, space-step, time-step, velocity and diffusion coefficient, in terms of two free parameters, the dimensionless Courant and Péclet numbers. Some performance criteria may be derived theoretically, and any criteria may be derived experimentally by searching the two-dimensional space comprising the ranges of these parameters. The nonlinearity of the CDE reported by *Richards* (1931) necessarily requires scaling in terms of at least three parameters, and comprehensively searching a space with corresponding dimensions.

There are two requirements for providing *a priori* guarantees of numerical performance for a nonlinear CDE. Firstly, the equation must be scalable in terms of a small number of parameters, so that it is practical to search the entire parameter space. Secondly, the properties of the nonlinear functions must allow the solution of the differential and finite difference equations to be determinate under all initial and boundary conditions.

With most soil hydraulic models, solutions must be represented in terms of numerous parameters: space-step, time-step, various soil hydraulic parameters and rainfall. The dimensionality of the parameter space may be reduced to three, using the soil hydraulic model (BW) of *Broadbridge and White* (1988). They pointed out that their model permitted scaling of soil hydraulic functions, Richards' equation, and initial and boundary conditions for rainfall infiltration, in terms of linear transformations of space, time and rainfall rate. Thus solutions could be scaled in terms of three parameters across all soils represented by the model. Another feature of this model is incorporation of *Fujita's* (1952) diffusivity function, which ensures that diffusivity remains finite as soil becomes very dry. This ensures that solutions of Richards' equation remain physically meaningful and determinate under all unsaturated conditions.

The BW soil hydraulic model has five parameters, each field measurable and having physical meaning. Four of these are related linear scaling factors, and the fifth embodies the nonlinearity of the hydraulic properties. This model appears to span a wide range of the known behaviour of field soils, ranging from highly to weakly nonlinear.

The range of nonlinearity of the BW soil model, combined with the ability to scale solutions in terms of three parameters, offers the prospect of guaranteed numerical performance in modelling a wide range of soils. We will demonstrate this using a particularly efficient numerical scheme, which can be readily incorporated into routine models of vertical soil-water dynamics. In the search for a suitable numerical scheme, a prime criterion is *Philip's* (1957a) principle of using exact global mass balance, which helps to constrain errors in approximate solutions, and also balances mass for simple water balance models having low accuracy requirements.

In this work we first discuss formulations of Richards' equation, then discuss requirements for determinacy of solutions. The BW soil model is examined and the range of analytical solutions (*Broadbridge and White*, 1988; *Broadbridge et al.*, 1988) is presented in a readily usable form. We present precise requirements for exact mass balance, and modify a particularly efficient mass-conserving numerical scheme investigated by *Ross* (1990). We compare analytical and numerical solutions for infiltration into extremely dry soil, using unusually large and fixed depth and time steps. For these conditions we develop criteria for guaranteed numerical convergence and stability.

4.9.2 Formulation of the flow equation

We restrict our attention to one-dimensional vertical soil-water flow, and assume that the soil is homogeneous, structurally stable, incompressible, isothermal and nonhysteretic. We will not consider here sources and sinks of water within the soil profile.

The term 'saturation' is somewhat misleading compared with 'satiation' (*Miller and Bresler*, 1977). For $\psi > 0$ some air is normally trapped within the soil pore space, so that even after the development of surface ponding or a watertable, θ increases slightly as ψ increases further.

Forms of the flow equation

The starting point in deriving the flow equation is conservation of mass for water flow in soil (*Gardner*, 1919):

$$\frac{\partial \theta}{\partial t} = -\frac{\partial q}{\partial z} \tag{4.1}$$

Nomenclature

z	depth below soil surface, +ve downwards [L]
t	time [T]
θ	volumetric soil-water content [$L^3\ L^{-3}$]
ψ	matric potential (pressure head) [L]
$K(\psi)$	hydraulic conductivity [$L\ T^{-1}$]
	soil-water diffusivity [$L^2\ T^{-1}$]
$D(\theta)$	$D = K\,\partial\psi/\partial\theta$
	D is also used in reference to linear CDEs
θ'	differential moisture capacity [L^{-1}] $\theta' = \partial\theta/\partial\psi$
K'	$\partial K/\partial\psi\ [T^{-1}]$
U	Kirchhoff transform, or matric flux potential [$L^2\ T^{-1}$] $U = \int_{-\infty}^{\psi} K\,d\psi = \int_{0}^{\theta} D\,d\theta$
q	soil-water flux in z-direction [$L^3\ L^{-2}\ T^{-1}$]
v	convective component of soil-water or solute flux [$L\ T^{-1}$]
P_e	Péclet number [dimensionless] $P_e = v\,\Delta z / D$
C_o	Courant number [dimensionless] $C_o = v\,\Delta t / \Delta z$

Subscripts and superscripts:

b	backward difference
f	forward difference
c	central difference
i	initial value
j	beginning of time-step for numerical solution
$j + 1$	end of time-step
0	soil surface
m	lower boundary
$*$	dimensionless form of variable, except that Θ is used for the dimensionless form of θ
$\ddagger$	form of variable with soil-independent scaling (see section 4.9.4)
s	the point at which soil becomes ‘saturated’, $\psi = 0$
r	residual moisture, using simplification $\theta \to \theta_r$ as $\psi \to -\infty$

Gardner derived a flow equation by substituting into (4.1) an expression for q developed for an 'ideal' soil. *Gardner* (1920) and *Gardner and Widtsoe* (1921) also clarified the meaning of *Buckingham's* (1907) potentials (matric and total), giving Buckingham's expressions for q the meaning:

$$q = K\left(1 - \frac{\partial \psi}{\partial z}\right) = K - D\frac{\partial \theta}{\partial z} \tag{4.2}$$

Richards (1931) substituted the first form of (4.2) into (4.1) and used differential moisture capacity $\theta' = \partial\theta/\partial\psi$, to obtain (in one-dimensional form) the flow equations:

$$\frac{\partial \theta}{\partial t} = -\frac{\partial}{\partial z}\left(K - K\frac{\partial \psi}{\partial z}\right) \tag{4.3}$$

$$\theta'\frac{\partial \psi}{\partial t} = -\frac{\partial}{\partial z}\left(K - K\frac{\partial \psi}{\partial z}\right) \tag{4.4}$$

These equations have great generality for describing non-hysteretic flow in soils, as the only constraint on soil properties proposed by Richards was that the hydraulic function $\psi(\theta)$ should be strictly monotonic.

Richards used equation (4.4) with ψ as the sole dependent variable, to derive an analytical solution, but proposed that one was free to choose either θ or ψ as the dependent variable. Richards suggested that 'mathematical expediency' should be the criterion for choosing the dependent variable. In the case of θ, the flow equation is derived very simply by substituting the second form of (4.2) into (4.1), giving:

$$\frac{\partial \theta}{\partial t} = -\frac{\partial}{\partial z}\left(K - D\frac{\partial \theta}{\partial z}\right) \tag{4.5}$$

Equation (4.5) was used by *Childs and Collis-George* (1950) and solved numerically by *Klute* (1952). Equations (4.4) and (4.5) are both highly nonlinear, since K, θ' and D are normally highly nonlinear functions of ψ.

Brutsaert (1971) extended the freedom to choose formulations as proposed by Richards, by solving (4.3), which has mixed dependent variables, using a finite difference technique. The use of a mixture of dependent variables means also that there is no fundamental distinction between dependent variables and nonlinear soil hydraulic functions such as θ', K, and D. Brutsaert used coarse node spacings Δz and Δt for a fairly general case involving satiated and layered soils, and highly nonlinear soil properties.

Other forms of the flow equation have been investigated with a view to dealing with its nonlinearity. *Haverkamp et al.* (1977) formulated the equation with Kirchhoff transform U as the sole dependent variable, giving:

$$\frac{\theta'}{K}\frac{\partial U}{\partial t} = -\frac{\partial}{\partial z}\left(K - \frac{\partial U}{\partial z}\right) \tag{4.6}$$

This linearises the diffusive term of the nonlinear convective-diffusive equation. However, the time derivative and the convective term $-\partial K/\partial z$ in (4.6) remain highly nonlinear. In fact, lower numerical efficiency was found than when solving (4.4). Others, (e.g. *Redinger et. al.*, 1984; *Campbell*, 1985), have applied the transform (*Gardner*, 1958) to just the diffusive term of (4.3), so that it becomes:

$$\frac{\partial \theta}{\partial t} = -\frac{\partial}{\partial z}\left(K - \frac{\partial U}{\partial z}\right) \tag{4.7}$$

with linear diffusive term and temporal derivative. *Ross* (1990) and *Ross and Bristow* (1990), using a finite difference scheme, found that solving (4.7) increased computational speed by an order of magnitude over solving (4.3), for a test case, and more than a further order of magnitude over solving (4.4). However, linearising individual terms of the differential equation for soil-water flow in no way changes the non-linearity of the soil functions or the flow problem. Because of this, and the success of *Brutsaert* (1971) in solving (4.3), it cannot be assumed that (4.7) will yield greater numerical efficiency than (4.3) for all rainfalls and the forms of the functions used in all soil hydraulic models.

Formulation as a convective-diffusive equation (CDE)

CDEs are generally used to model transport of solutes moving with liquids. For one-dimensional flows the form is:

$$\frac{\partial C}{\partial t} = -\frac{\partial}{\partial z}\left(vC - D\frac{\partial C}{\partial z}\right) \tag{4.8}$$

where C is solute concentration and v fluid velocity. Equation (4.5) has this form with: θ interpreted as concentration of water in the soil by volume, diffusivity interpreted in the usual way, and velocity v interpreted as K/θ.

Recognising that residual soil-water ($\psi \to -\infty$) is immobile, an appropriate refinement is the definition $v = K / (\theta - \theta_r)$. This has two advantages. Firstly, the increase in velocity makes claims

later in this work conservative, regarding dominance of diffusion over convection in soil-water flows. Secondly, this definition is consistent with use of the dimensionless forms of K and θ, *viz.* K^* and Θ, defined in Table 4.4 and used in various soil hydraulic models. The dimensionless Péclet and Courant numbers, P_e and C_o, have been used widely to investigate the performance of numerical schemes for solving linear CDEs; the definitions are given earlier. *Noye* (1990) discussed various finite difference representations of a linear CDE, having four parameters: v, D, Δz and Δt. The equations were scaled in terms of two independent parameters using C_o and a dimensionless diffusion number, with P_e implicit. Numerical stability was unconditional for $C_o = 1$ and $P_e = 2$ for a range of difference schemes. The parameter C_o is the magnitude of v relative to the length and time scales Δz and Δt, with values >> 1 requiring specialised numerical techniques. P_e represents relative dominance of convective components of flux over diffusive components relative to the length scale.

For soils and with dimensionless variables, which do not affect the meanings of these numbers (see Table 4.4), the definitions earlier yield:

$$P_e = \frac{1}{\Theta}\frac{\Delta\Theta}{\Delta\psi^*}\Delta z^* \tag{4.9}$$

$$C_o = \frac{K^*}{\Theta}\frac{\Delta t^*}{\Delta z^*} \tag{4.10}$$

It should be noted that effectively using a dimensionless form of (4.5) to formulate P_e and C_o does not constrain the choice of form of Richards' equation for numerical solution.

Recent studies (*El-Kadi and Ling*, 1993; *Huang et al.*, 1994) have considered P_e and C_o, at least implicitly, in studying numerical solutions of the nonlinear CDE for soil-water flow. It was assumed that at each point in space and time, P_e and C_o criteria based on local soil-water content could be developed for infiltration into semi-infinite soil profiles. In the special case of a region with relatively uniform θ-values, criteria developed for linear CDEs could be expected to apply directly.

We disagree with the last mentioned authors regarding the form of Richards' equation that may be interpreted as a CDE. *El-Kadi and Ling* (1993) transformed (4.6) into a CDE with dependent variable U. Convective term v was defined using the incorrect assumption $\partial/\partial z\ (vU) = v\ \partial U/\partial z$. It appears that Richards' equation cannot be formulated consistently as a mathematical CDE in U. Perhaps more importantly, it is inappropriate to formulate P_e and C_o using mathematical convection and diffusion of an intensive (intensity or potential) variable such as U (*El-Kadi and Ling*, 1993) or ψ (*Huang et al.*, 1994), rather than extensive (content) variables like θ or Θ. Specifi-

cally, intensive variables give no physical meaning to the concepts of convection and diffusion. Therefore they cannot yield direct insight into the relative roles of convection and diffusion of soil water content. Further, with such variables, we cannot meaningfully compare numerical performance criteria with those for linear CDEs.

Finally, we pose the question as to whether P_e and C_o values ever need to be high enough to cause numerical problems for rainfall infiltration, or other unconfined aquifer soil-water dynamics. For the traditionally difficult case of infiltration into extremely dry soil ($\psi \rightarrow -\infty$), we found essentially zero values of P_e and C_o as represented by the soil hydraulic models of *Campbell* (1974) and *Broadbridge and White* (1988). With these models, numerical infiltration should be extremely easy at the leading edge of the wetting front, as far as P_e and C_o values are concerned, as the problem is completely diffusion-dominated. This situation is to be expected for any soil model that is physically realistic for very dry conditions, because water movement is primarily in the vapour phase, for which convection due to gravity is irrelevant.

In the case of satiated soil, $K^* \cong \Theta \cong 1$, so that $C_o = \Delta t^* / \Delta z^*$, permitting large node spacings. Further $\partial\Theta / \partial\psi^* \cong 0$, so $P_e \cong 0$; again the problem is nearly completely diffusion dominated if the soil hydraulic model is physically realistic. In this case Richards' equation approximates a linear CDE, so that numerical convergence and stability are obtained very easily. For intermediate soil-water contents, *Philip* (1993) justified the assumption of diffusion-dominated flow in deriving an approximate solution.

4.9.3 Determinacy of solutions of the flow equation

Performance of numerical solution techniques cannot be guaranteed unless solutions of both the differential and finite difference equations are always determinate, that is, exact and unique solutions must exist under all conditions. Further, the finite difference equations must be solvable using practical techniques. In part, these requirements impose constraints on the forms of the soil hydraulic functions. We will examine the adequacy of *Richards'* (1931) constraint that $\psi(\theta)$ is strictly monotonic.

Existence of solutions in very dry soil

Philip (1957b) recognised that vapour diffusion makes D finite in extremely dry soil, but proposed the simplification that $D = K\partial\psi/\partial\theta \rightarrow 0$ as $\psi \rightarrow -\infty$, in developing quasi-analytical solutions. *Philip* (1992) and *Philip and Knight* (1991) obtained analytical solutions using the same simplification for cases where $D(\theta)$ and $\partial K/\partial\theta$ were represented by power law functions. Exact solutions of the flow equation exist for $D = 0$ with arbitrary 'well behaved' soil functions, for

prescribed flux boundary conditions. Zero D makes gradients $\partial\theta/\partial z, \partial\theta/\partial t$, $\partial D/\partial z$, etc, infinite. The solution has these physically implausible properties at the soil surface, for an infinitesimal value of *t*, and over an infinitesimal region at the leading edge of the wetting front for all finite *t*.

Because these singular regions are infinitesimal, analytical solutions are determinate, but problems arise in finding numerical solutions. Firstly, solutions of the finite difference equations do not exist, in general, if the initial estimate of Θ is zero at any space node. Numerical difficulty must be expected when this condition is approached closely. Secondly, it is impractical to change the modelled region continually to avoid dry regions. Thirdly, if strategies are devised to obtain solutions for specific numerical schemes, no finite degree of reduction of depth node spacing Δz can cause numerical solutions to converge toward exact solutions. Finally, the infinite gradients in the singular regions will be approximated in finite difference solutions by very large gradients. These, combined with finite fluxes, may cause the numerical problems normally associated with convection-dominated flows.

Richards' (1931) requirement, that $\psi(\theta)$ should be strictly monotonic, is sufficient to prevent $\partial\psi/\partial\theta$ from becoming infinite at finite values of ψ. This is physically reasonable, and assures non-zero values of $\partial\theta/\partial\psi$ as required, for example, by Newton–Raphson numerical solution schemes (see section 4.9.6). However, for numerical schemes a weak additional constraint should be imposed on *K* or *D*, so that $D = K\partial\psi/\partial\theta$ remains finite; this requirement is met by the hydraulic model of *Broadbridge and White* (1988).

Widely used soil models such as those of *Campbell* (1974) and *van Genuchten* (1980) do not meet this requirement. For water balance modelling purposes the formulation of *D* in dry soils is irrelevant, as the quantities of water that may be distributed inaccurately by a solution are very small. However, numerical models require strategies for coping with zero *D*, otherwise numerical performance cannot be guaranteed.

Uniqueness of solutions in satiated soils

In satiated soils, *Richards'* (1931) requirement of strictly monotonic $\psi(\theta)$ yields unique solutions. This is because $\partial\theta/\partial\psi$ remains non-zero, in keeping with air entrapment and compression in 'saturated' soils. This ensures that *D* remains finite, regardless of whether $\partial K/\partial\psi$ is assumed to be small, or zero in accordance with common practice. A unique exact solution of (4.5) therefore exists.

Most soil hydraulic models set $\partial\theta/\partial\psi = 0$ in the satiated range of ψ. This range may be $\psi = 0$, or $\psi = \psi_a$, where ψ_a (negative) is the 'air-entry' potential. A moisture characteristic, $\psi(\theta)$, for the

latter case is shown in Fig. 4.2, for the soil model of *Campbell* (1974). For this model $\partial\theta/\partial\psi = 0$ in the satiated range makes D infinite. A very high D does not pose numerical problems, but infinite D makes the solution indeterminate, and numerical problems may arise. These problems may be overcome by extending $\psi(\theta)$ monotonically through the satiated range. This is very simple for the model of *Broadbridge and White* (1988), as $\partial\theta/\partial\psi$ is finite at $\psi = 0$. This condition does not hold for most other models, so that additional parameters may be needed.

The problem of determinacy in satiated soil has been partly addressed previously. It has been recognised (e.g. *Philip* 1958; *Haverkamp et al.*, 1977) that the usual practice of setting $\partial\theta/\partial\psi = 0$ in satiated soil makes the fluxes on the right hand side of (4.5) indeterminate. The proposed solution was to solve only (4.4). However, in (4.3) and (4.7) the fluxes are equally indeterminate with this assumption, although other workers (e.g. Brutsaert, 1971; *Ross and Bristow*, 1990) have solved these equations for satiated soil.

Nevertheless, the time course of solutions may be indeterminate. This can be illustrated by considering the redistribution of water in a soil profile with depth less than $-\psi_a$ and an impermeable lower boundary. When the whole system is satiated, the spatially uniform zero flux and the variation of ψ with depth are determinate. But because we also have $\partial\theta/\partial t = 0$, there is no way for a solution of the flow equation to determine actual values of ψ, or changes with time. In this situation the depth of the watertable ($\psi = 0$) may assume any value within the soil profile.

We investigated this case numerically for the Campbell soil model using the computer code provided by *Ross and Bristow* (P. J. Ross, personal communication, 1991). Fig. 4.3 shows simulated 'watertable' depth, expressed as $z/(-\psi_a)$, after one day's redistribution following a spatially uniform initial condition $\psi = \psi_a$. Each point represents a simulation with the soil profile discretised into the given number of depth nodes. The 'watertable' depth is chaotic, ranging over the whole soil depth. The gaps represent convergence failures, which are mostly associated with decimal values of Δz that have exact binary representations (e.g. 0.25). This is because, when the soil profile is full, the indeterminate problem posed by the differential equation, when using the Campbell soil model, requires solution of a mathematically singular matrix in the numerical scheme. Where the convergence occurred, computational round-off error obscured the singularity of the matrix.

This example was, of course, carefully chosen to demonstrate numerical failure. Two points must be stressed here. Firstly, this situation is likely to be encountered frequently by soil-water dynamics models used in a routine way; the soil profile or a soil layer will often be filled. Secondly, the overall numerical strategy of Ross and Bristow is very efficient, and indeterminacy arises from the properties of the soil hydraulic functions used.

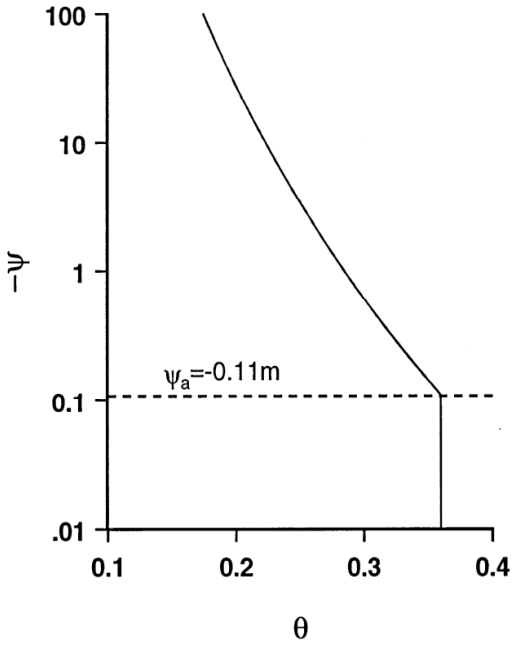

Fig. 4.2 : Example of a moisture characteristic, using the soil hydraulic model of Campbell (1974), showing $\partial\theta/\partial\psi=0$ for $\psi \geq \psi_a$, where ψ_a is the air-entry potential.

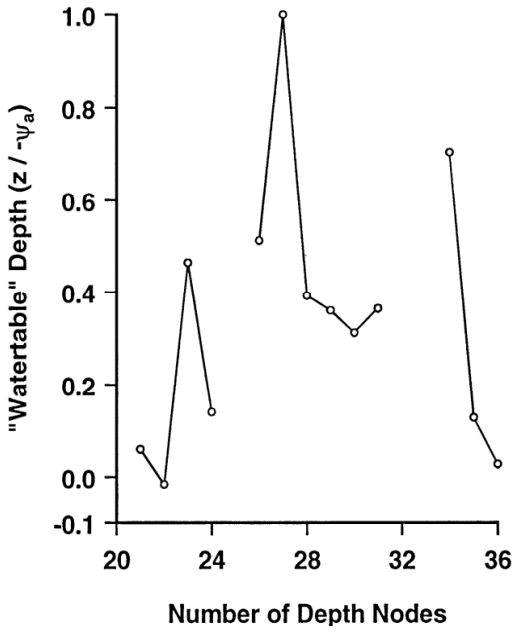

Fig. 4.3: Simulated watertable depths in 'tension-saturated' soil, plotted against the number of depth nodes into which a soil with depth $-\psi_a$ was discretised, using the Campbell soil hydraulic model. Gaps represent convergence failures.

There are precedents for adapting soil hydraulic models for finite $\partial\theta/\partial\psi$ in the satiated ψ-range. For example, *Paniconi et al.* (1991) used such a modification of the van Genuchten soil model, to prevent Richards' equation from becoming elliptical in multidimensional cases, and to overcome numerical problems found with two of the six numerical schemes they investigated for one-dimensional infiltration. We propose general use of this strategy, to permit guaranteeing numerical performance without imposing unnecessary constraints on the choice of numerical scheme.

4.9.4 Soil hydraulic model and analytical solutions

Broadbridge–White Soil Hydraulic Model

The model represents soil-water content up to the point of soil satiation (i.e. for $\psi \leq 0$). It encompasses a realistic range of moisture characteristics and $K(\psi)$, and is conceptually simple with physically identifiable parameters. There are five parameters:

θ_s volumetric soil-water content at satiation

θ_r residual soil-water content ($\psi \to -\infty$) we write $\Delta\theta = \theta_s - \theta_r$

K_s $K(\theta_s) = K(\psi_{=0})$, satiated hydraulic conductivity

$K_r = K(\theta_r)$, is normally assumed to be zero

λ_c macroscopic capillary length scale, a scaling length for space and soil moisture potential [L]

C a soil structure parameter, describing the degree of nonlinearity of the soil properties, and related to the slope of $\psi(\theta)$ as $\theta \to \theta_s$. As $C \to \infty$ the soil is weakly nonlinear, as $C \to 1$ the soil is highly nonlinear.

The first four parameters can be measured in the field or laboratory (*White and Broadbridge*, 1988). The parameter λ_c arises in many different contexts in soil-water flow (see e.g. *Raats and Gardner*, 1971; *White and Sully*, 1987). It is inversely proportional to a flow-weighted mean pore size and is also related to the matric flux potential, *U*. It is an appropriate scaling quantity for matric potential and for distance. The parameter *C* is related to the slope of the moisture characteristic at satiation. That is, it is related to the size distribution of the larger pores. The parameters θ_s, θ_r, K_s and λ_c are factors used to scale the fundamental variables θ, ψ, K into dimensionless variables Θ, Ψ^*, K^*. This yields linear scaling of all other hydraulic variables, flux (e.g. rainfall rate), space and time. The dimensionless variables are given in Table 4.4, with their relation to familiar dimensioned parameters, and the corresponding functional dependence assumed by the model, where appropriate. As well, the non-dimensional flux and rainfall are also shown.

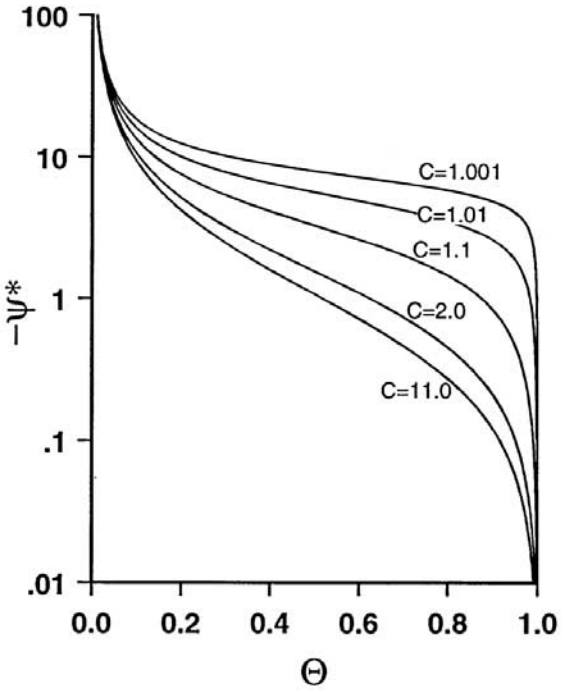

Fig. 4.4: Dimensionless moisture characteristics used in the BW soil hydraulic model, parameterized by the single soil parameter *C*.

Dimensionless functions assist in visualising the relationships between the hydraulic properties of all soils having the same nonlinearity. Dimensionless soil functions, and solutions of the flow equation, for a particular value of *C* are applicable to all soils with that value of *C* but possessing different K_s, λ_c, θ_s and θ_r. Fig. 4.4 shows dimensionless moisture characteristics, $\psi^*(\Theta)$, for selected values of *C*; the family of curves may be scaled to all soils represented by the model.

Table 4.4: Dimensionless variables for scaling BW soil hydraulic model

Scaling of Variable	Function
$\Theta = \frac{\theta - \theta_r}{\theta_s - \theta_r}$	
$\psi^* = \frac{\psi}{\lambda_c}$	$\psi^* = 1 - \frac{1}{\Theta} - \frac{1}{C} ln \frac{C - \Theta}{(C-1)\Theta}$
$K^* = \frac{K}{K_s}$	$K^* = \Theta^2 \frac{C-1}{C-\Theta}$
$D^* = \frac{D\, t_c}{\lambda_c^{\,2}}$	$D^* = \frac{C(C-1)}{(C-\Theta)^2}$
$U^* = \frac{U}{K_s\, \lambda_c}$	$U^* = \Theta \frac{C-1}{C-\Theta} = \frac{K^*}{\Theta}$
$\frac{\partial \Theta}{\partial \psi^*} = \frac{\partial \theta}{\partial \psi} \frac{\lambda_c}{\Delta \theta}$	$\frac{\partial \Theta}{\partial \psi^*} = \Theta^2 \frac{C-\Theta}{C}$
$\frac{\partial K^*}{\partial \psi^*} = \frac{\partial K}{\partial \psi} \frac{\lambda_c}{K_s}$	$\frac{\partial K}{\partial \psi^*} = \Theta^3 \frac{(C-1)(2C-\Theta)}{C(C-\Theta)}$
$t^* = \frac{t}{t_c}$	$t_c = \frac{\Delta\theta\, \lambda_c}{K_s}$
$z^* = \frac{z}{\lambda_c}$	
$R^* = \frac{R}{K_s}$	
$q^* = \frac{q}{K_s}$	
$v^* = \frac{v \Delta\theta}{K_s}$	$v^* = \frac{K^*}{\Theta} = U^*$
	$P_e = \frac{\Theta(C-\Theta)}{C} \Delta z^*$
	$C_o = \frac{\Theta(C-1)}{C-\Theta} \frac{\Delta t^*}{\Delta z^*} = U^* \frac{\Delta t^*}{\Delta z^*}$

Note that C is the only parameter in the model, and variables are functions of dimensionless water content Θ only. The functions are suitable for most practical modelling applications, providing reasonable approximations to known soil properties, along with a comprehensive range of non-linearity of soil behaviour.

To assist in relating the model to actual soils, we consider surface soils having two values of the soil structure parameter, C = 1.02 and C = 1.5. These values correspond to approximately the range found in the field (White and Broadbridge, 1988). The first soil is a rather unstructured sand, with highly nonlinear moisture characteristic: C = 1.02, θ_s = 0.4, θ_r = 0.05, K_s = 2.0 m d^{-1}, λ_c = 0.3 m, and $t_c = \lambda_c \Delta\theta / K_s$ = 0.052 d. The second, a structured surface soil, with weakly non-linear moisture characteristic, is represented by: C = 1.5, θ_s = 0.5, θ_r = 0.1, K_s = 1.0 m d^{-1}, λ_c = 0.1 m, and t_c = 0.04 d. A final example is a clay subsoil. Because of its fine texture, variability of soil particles yields a high value of the structure parameter, C = 2.0, in spite of the absence of macropores, and also a high length/potential scale parameter, λ_c = 2.0 m, and low hydraulic conductivity scale parameter, K_s = 0.01 m d^{-1}. With soil-water content scaled by θ_s = 0.4 and θ_r = 0.15, the time scale becomes t_c = 50 d.

Functional forms of P_e and C_o given in Table 4.4 were derived by substituting soil model functions into (4.9) and (4.10). $C_o \le \Theta \, \Delta t^*/\Delta z^*$ for all $\Theta \le 1$, so that the condition $C_o \le 1$ is always met if $\Delta z^* > \Delta t^*$. $P_e \le \Theta \, \Delta z^*$ for all $\Theta \le 1$, so that the condition $P_e \le 2$ is always met if $\Delta z^* \le 2$. Translating these criteria to dimensioned variables, we have $\Delta z \le 2 \, \lambda_c$ with $\Delta t \le 2 \, t_c$. Referring back to the three soil examples, we see that direct application of P_e and C_o criteria for linear CDEs to soil-water flows would permit unusually large node spacings, that is, Δz at least a large fraction of a metre with Δt over 1 hour, for numerical stability, even for the surface soils.

Numerical solutions remain determinate as $\Theta \to 0$, as D^* has the small but finite value $(C–1)/C$. As $\Theta \to 1$, D^* approaches the large but finite value $C/(C–1)$. To retain determinacy for $\psi \to 0$, it is necessary to extend $\Theta(\psi)$, $D(\psi)$ and $K(\psi)$ monotonically from $\psi = 0$. Two things follow from the BW soil model's feature that $\partial\theta/\partial\psi$ is finite for $\psi = 0$. It allows monotonicity to be achieved very simply, without modification within the model's original unsatiated range. However, it also makes monotonicity mandatory, because if $\partial\theta/\partial\psi = 0$ for $\psi > 0$, numerical convergence is normally unobtainable, whereas when $\partial\theta/\partial\psi = 0$ for $\psi > \psi_a$, convergence is obtained in many cases.

In this work, dimensionless numerical simulations will solve a dimensionless form of (4.7):

$$\frac{\partial \Theta}{\partial t^*} = -\frac{\partial}{\partial z^*}\left(K^* - \frac{\partial U^*}{\partial z^*} \right) \tag{4.11}$$

Scaling the soil model and flow equation across all soils

Broadbridge and White (1988) pointed out that further scaling of their model made variables and solutions of the flow equation independent of C, that is, scaling could be performed across all soils represented by the model. This is achieved by using Θ/C, $C\psi^*$ and $K^*/(4C(C-1))$, to transform soil-water content, potential and hydraulic conductivity, respectively, to 'universally scaled' variables, which we shall represent by the superscript '‡'.

Table 4.5 shows the universally scaled functions, variables and fluxes, analogous to Table 4.4. The functions, which represent all soils, involve no parameters. All the information in Table 4.4 is embodied here, however, apart from an arbitrary constant in the expression for $\psi^{\ddagger}$. To scale functions to a particular soil, we require the condition $\Theta^{\ddagger} = 1/C$, so that the model is still used only up to the point of satiation. For satiated cases, it is not feasible to scale across all soils, although the quasi-linearity of satiated soil hydraulics makes this case simple numerically.

Comparing the forms of P_e and C_o with those of Table 4.4, we see that for given dimensioned parameter values, these numbers are not changed by the further scaling. However since the form of P_e in Table 4.5 is independent of C, we can avoid the global inequality used earlier. Then the condition $P_e \le 2$ yields a less conservative upper limit for Δz, *viz.* $8\,\lambda_c/C$.

Table 4.5: Universal dimensionless variables for scaling BW soil hydraulic model

Universal Function	Universal Function
$\Theta^{\ddagger} = \dfrac{\Theta}{C}$	$\psi^{\ddagger} = \psi^* C$
$m = 4C(C-1)$	$K^{\ddagger} = \dfrac{K^*}{m}$
$D^{\ddagger} = D^* \dfrac{C^2}{m}$	$U^{\ddagger} = U^* \dfrac{C}{m}$
$\dfrac{\partial \Theta^{\ddagger}}{\partial \psi^{\ddagger}} = \dfrac{\partial \Theta}{\partial \psi^*} \dfrac{1}{C}$	$\dfrac{\partial K^{\ddagger}}{\partial \psi^{\ddagger}} = \dfrac{\partial K}{\partial \psi^*} \dfrac{1}{C\,m}$
$z^{\ddagger} = z^* C$	$\tau = t^* m$
$\rho = \dfrac{R^*}{m}$	$q^{\ddagger} = \dfrac{q^*}{m}$
$P_e^{\ddagger} = \Theta^{\ddagger}\left(1-\Theta^{\ddagger}\right)\Delta z^{\ddagger}$	$C_o^{\ddagger} = \dfrac{\Theta^{\ddagger}}{4\left(1-\Theta^{\ddagger}\right)} \dfrac{\Delta\tau}{\Delta z^{\ddagger}}$

The universally scaled hydraulic functions are even more powerful than those of the original form of the soil model, for expressing physical relationships between cases. They meet our requirement for a tool for comprehensively investigating and predicting numerical performance. In terms of the universally scaled variables, flow equation (4.7) becomes:

$$\frac{\partial \Theta^{\ddagger}}{\partial \tau} = -\frac{\partial}{\partial z^{\ddagger}}\left(K^{\ddagger} - \frac{\partial U^{\ddagger}}{\partial z^{\ddagger}} \right) \tag{4.12}$$

Analytical solutions

For comparison with numerical solutions we consider analytical solutions for constant vertical flux into semi-infinite and finite depth columns of uniform soil, with both zero and finite initial soil-water content, whose hydraulic properties are described by the BW model. The dimensionless analytical solutions corresponding to the original form of the soil model for constant flux infiltration up to the point of surface satiation are:

$$\frac{\Theta}{C} = 1 - \frac{1}{2\rho + 1 - (\partial u/\partial \zeta)/u} \tag{4.13}$$

$$C\, z^{*} = \rho(\rho + 1)\tau + (2\rho + 1)\zeta - \ln u \tag{4.14}$$

where u is a function of initial and boundary conditions and is given in Appendix B. It can be seen from the structure of (4.13) and (4.14) that these solutions may be transformed to universally scaled exact solutions of the flow equation, using the universally scaled variables Θ/C, Cz^{*} and ρ.

For a semi-infinite profile with zero initial soil-water content, u is a function of ζ, τ and ρ, which are space, time and rainfall variables resulting from transformations that linearise the flow equation (*Broadbridge and White*, 1988). For a finite-depth profile with zero initial soil-water content, $u = u(\zeta, \tau, \rho, C\, l^{*})$, where $l^{*} = l / \lambda_c$ is the dimensionless depth of the soil profile (*Broadbridge et al.*, 1988). For finite initial soil-water content Θ_i, in either semi-infinite or finite depth soils, u becomes a function of Θ_i also (*Broadbridge*, 1990). Expressions for u and $\partial u/\partial \zeta$ for these cases are presented in Appendix B. Numerical problems can be encountered in computing the analytical solutions. Precautions to ensure the accuracy of analytical solutions presented in this paper are explained in Appendix B.

Universal scaling does not depend on the existence of analytical solutions. The latter are used because of the soil model's considerable degree of realism (*White and Broadbridge*, 1988), and to illustrate the accuracy obtainable with universally scaled numerical solutions with large practical node spacing. Universal scaling may not depend on the particular functional forms of the BW soil

model. However, it is desirable for any future approach to universal scaling to ensure determinacy of solutions of Richards' equation, and to address the question of diffusion-dominance of soil-water flow.

4.9.5 Exact mass balance in finite difference solutions

The immediate aim of this work is to show that an approach to soil hydraulic modelling, which gives determinacy and scaling of solutions, achieves the completely predictable numerical performance required for routine use in practical models. Predictability could be demonstrated using any numerical scheme, using in particular, any form of the flow equation. However, we propose to demonstrate predictable performance using the numerical advantages of exactly mass-conserving schemes.

It must be stressed that all forms of the differential equation are analytically equivalent, and incorporate the mass conservation of (4.1), so that exact solutions must balance mass exactly. We are concerned here with retaining this feature in spite of the approximations involved in using finite difference solution techniques. We do not distinguish in this context between 'finite difference' and 'finite element' methods for devising the finite difference representation of the differential flow equation.

In practical modelling applications mass should be conserved accurately, even when there are low accuracy requirements for determining soil-water distribution. Further, for more demanding applications, exact global mass balance necessarily imposes constraints on errors. In particular, this constrains propagation of the substantial errors that necessarily occur shortly after infiltration begins, if using relatively large uniform Δz and Δt. Likewise, numerical instabilities are constrained.

Philip (1957a) proposed exact global mass balance to constrain errors in quasi-analytical solutions, using the divergence theorem of vector calculus. This theorem says that the surface integral of flux of into a region across its boundaries, equals the volume integral of the rate of increase in content over the region, provided that it contains no sources or sinks. Exact mass balance has been long used in finite difference solutions in fluid mechanics (see e.g. *Roache*, 1976), by generalising the divergence theorem to arbitrary finite space and time steps.

Exact mass balance has been reported also in finite difference solutions of Richards' equation or the related nonlinear diffusive equation for horizontal soil-water flow (see e.g. *Hornung and Messing*, 1981; *Ross*, 1990; *Celia et al.*, 1990). In these works two fundamental requirements are clear, (a) the flow equation must be a form using $\partial\theta/\partial t$ as the temporal derivative, for example, equations (4.3), (4.5) and (4.7), and (b) exact mass accounting requires linear interpolation of θ

between space nodes, i.e. trapezoidal integration of mass. Further, this result may be obtained for all boundary conditions, as recognised by *Celia et al.* (1990), and demonstrated in the computer code of *Ross and Bristow* (P. J. Ross, personal communication).

We now set out precise requirements for mass-conservative finite differencing, using the short-hand notation of a finite difference representation of continuity equation (4.1). It is important not to impose any unnecessary constraints on the choice of numerical scheme.

Equation (4.1) in finite difference form is, at an internal depth node:

$$F_i = \alpha\left(q_{i+0.5}^{j+1} - q_{i-0.5}^{j+1}\right) + (1-\alpha)\left(q_{i+0.5}^{j} - q_{i-0.5}^{j}\right) + e_i = 0 \tag{4.15}$$

with $$e_i = \left(\theta_i^{j+1} - \theta_i^{j}\right)\Delta z_{ci} / \Delta t_{fj} \tag{4.16}$$

Here $q_{i+0.5}$ is soil-water flux at the midpoint between depth nodes i and $i+1$, $\Delta z_{ci} = (\Delta z_{fi} + \Delta z_{fi-1})/2$, Δt_{fj} is size of the time-step beginning at time j, and α is the temporal weighting of the spatial differential. At the upper and lower boundaries, we use simple non-centred differences in space over the top and bottom half node spacings. The difference equations at the upper and lower boundaries are respectively:

$$F_0 = \alpha\left(q_{0.5}^{j+1} - q_0^{j+1}\right) + (1-\alpha)\left(q_{0.5}^{j} - q_0^{j}\right) + e_0 = 0 \tag{4.17}$$

$$F_m = \alpha\left(q_m^{j+1} - q_{m-0.5}^{j+1}\right) + (1-\alpha)\left(q_m^{j} - q_{m-0.5}^{j}\right) + e_m = 0 \tag{4.18}$$

where the boundary e-values are calculated using $\Delta z_0 = \Delta z_{f0}/2$ and $\Delta z_m = \Delta z_{bm}/2 = \Delta z_{fm-1}/2$. Summing F_i over all depth nodes, all internal q's cancel, leaving boundary fluxes. Multiplying by Δt and rearranging, we have:

$$\begin{aligned}\sum_{i=0}^{m} F\,\Delta t = {} & \Delta t\left(\alpha q_m^{j+1} + (1-\alpha) q_m^{j}\right) - \Delta t\left(\alpha q_0^{j+1} + (1-\alpha) q_0^{j}\right) + \\ & \sum_{i=0}^{m-1}\left(\theta_{i+1}^{j+1} + \theta_i^{j+1}\right)\Delta z_{fi}/2 - \sum_{i=0}^{m-1}\left(\theta_{i+1}^{j} + \theta_i^{j}\right)\Delta z_{fi}/2 = 0\end{aligned} \tag{4.19}$$

The four terms on the right hand side of (4.19) for a single time-step are, in order: cumulative flux of water at the lower boundary; cumulative flux at the upper boundary; final soil-water content in the profile; and initial soil-water content in the profile. Equation (4.19) expresses mass balance over the time-step Δt, provided that soil-water content in the profile is obtained by trapezoidal integration of θ. Also, when fluxes vary in time, the cumulative boundary fluxes are computed by integration of q using the same temporal weighting as in the difference equation.

If mass balances exactly over one time-step, it also balances exactly over an arbitrary number of time-steps. Summing (4.19) over N time-steps from $j = 0$ to $j = N$, and cancelling profile contents at intermediate times, we obtain the corresponding exact mass balance for the duration of a simulation:

$$\sum_{j=0}^{N-1}\sum_{i=0}^{m} F_i \Delta t^j = \sum_{j=0}^{N-1} \Delta t^j \left(\alpha q_m^{j+1} + (1-\alpha) q_m^j\right) - \sum_{j=0}^{N-1} \Delta t^j \left(\alpha q_0^{j+1} + (1-\alpha) q_0^j\right) + \sum_{i=0}^{m-1} \left(\theta_{i+1}^N + \theta_i^N\right) \Delta z_{fi} / 2 - \sum_{i=0}^{m-1} \left(\theta_{i+1}^0 + \theta_i^0\right) \Delta z_{fi} / 2 = 0 \tag{4.20}$$

The above result holds, irrespective of whether boundary fluxes are prescribed in advance, or are determined by gravity drainage with $\partial\psi/\partial z = 0$ at the lower boundary. It also holds for potential boundary conditions, since (4.17) and (4.18) still contribute to mass balance, although they are no longer used in obtaining the solution.

Potential boundary conditions, however, do cause two complications. For a prescribed condition at the surface, the first complication is that in order to preserve mass balance, it is necessary to set $q_0 = q_{0.5}$, at time j or $j+1$. This is because fixed surface potential ψ_0 sets $e_0 = 0$ in (4.17). While this may be intuitively unsatisfying, the cost of a more sophisticated relationship between q_0 and $q_{0.5}$ is a loss of mass balance. The second complication is that, in general, there is a transient contradiction between a given moisture profile at time j and a potential boundary condition introduced at the same time. Imposing ψ_0 entails an instantaneous change in θ_0, and requires a corresponding change in profile moisture content of $0.5\,(\theta_{0,new} - \theta_{0,old})\,\Delta z_{f0}$, for exact mass accounting.

The cancellation of all internal fluxes and intermediate profile soil-water contents, implicit in (4.20), achieves exact mass balance for a wide range of situations. The first is arbitrary spatial arrangement of depth nodes and arbitrary variation of time node spacing. The second is any method of estimating midpoint hydraulic conductivity (e.g. arithmetic, geometric or harmonic mean). The third is any representation of θ, for example, in terms of θ, ψ or U. The fourth condition is arbitrary spatial and temporal variation in the formulation of q. Even completely arbitrary internal fluxes must cancel, provided only that flux at a given point in space and time is the same for the two times it is computed.

The generality of (4.20) may be extended further, to spatial weighting of temporal differentials, provided that precisely the sum of the e-values of (4.16) is distributed among all the depth nodes. For example, the Douglas finite difference scheme (e.g. *Mitchell*, 1969) meets this condition.

There are constraints on direct use of finite element techniques in mass-conservative schemes. For example, a finite element scheme with piecewise linear basis functions and a consistent time

matrix, which was investigated by *Celia et al.* (1990), does not conserve mass exactly for spatially variable Δz, although this is nearly the same as the Douglas finite difference scheme. Also, direct use of finite element techniques with higher-order differencing in space is inconsistent with the requirement for linear spatial interpolation of θ for mass accounting. If this requirement is met, higher-order finite difference equations, which have been used in pursuit of more accurate solutions (e.g. *Chaudhari*, 1971; *Bresler*, 1973), will conserve mass.

Mass will not be conserved for flux boundary conditions if the flux is represented in finite difference form, instead of simply being prescribed (see e.g. *Whisler and Klute*, 1967; *Haverkamp and Vauclin*, 1981; *Wallach and Shabtai*, 1992). A finite difference representation of surface flux q_0, involves setting up unknown potential ψ_{-1} at a conceptual node just outside the boundary, expressing q_0 in terms of central differences at $i = 0$, and using the prescribed value of θ_0 to eliminate ψ_{-1}. This causes mass balance error in two ways, when the F_i are summed. Firstly, e_0 in equation (4.17) uses double the correct Δz value, so that spurious soil-water outside the boundary is included in the summation. Secondly, the flux not cancelled by the summation is $\theta_{-0.5}$ instead of the boundary flux θ_0.

In this work we have found that this treatment of the boundary flux imposed very severe Δz and Δt constraints in numerical solutions of (4.4) for any reasonable mass balance. It required, for example, $\Delta z_0 << 1$ mm, to achieve cumulative surface flux errors in mass balance of 1 part in 100 for rainfall and 1 part in 5 for evaporation.

The final requirement for mass conservation is a mass-conserving criterion for convergence of the solution at the end of each time-step. This criterion is the convergence of the vector $[F_i]$ to nearly zero (*Ross*, 1990). With a complete mass-conservative numerical scheme, mass accounting requires only trivial computational effort. The change in global mass balance over the time-step is simply the sum of F_i over all depth nodes. If a potential boundary condition has been introduced at the beginning of the current time-step, then the correction described above must be used as well.

In this work, we use a convergence criterion of $|F_i| < 10^{-10}$, and mass balance errors in cumulative infiltration are less than one part in 10^{11} for all simulations reported.

4.9.6 Numerical scheme

Choosing the numerical scheme

A flow problem that is generally regarded as numerically difficult is high-rate infiltration into very dry soil. Depending on choice of numerical scheme and soil hydraulic functions, computa-

tional effort for a single infiltration event of this type may range from hundreds of seconds on a highly configured supercomputer (e.g. *Paniconi et al.*, 1991), to a few seconds on a personal computer (IBM PC-AT) having low performance by current standards (e.g. *Ross*, 1990).

We seek a numerical strategy that is known to be computationally efficient and conserves mass exactly, and this will be used with the hydraulic functions that permit guaranteed numerical performance. A literature search suggested the following features: use of (4.7) as the form of the flow equation, the simple finite differencing described in section 4.9.5, a Newton–Raphson iterative scheme for solving the finite difference equations, and the simplest possible initial estimate of the solution for the current time-step, *viz.* the solution for the previous time-step. We note that all these features are to be found in the work of *Ross and Bristow* (1990). Our numerical solutions of (4.3), (4.4) and (4.7), including comparisons of Newton–Raphson and Picard solution schemes and comparisons of the BW and Campbell soil models, confirmed this choice as appropriate for the range of infiltration events studied. However, we found advantages in changing some details of the numerical strategy of Ross and Bristow.

We found some convergence problems with the computer code of *Ross and Bristow* (1990), occurring unexpectedly within parameter ranges that generally seemed reliable. For example, for infiltration into their 'sand' with initial condition $\psi = -351$ m, and node spacing $\Delta z = 0.0625$ m and $\Delta t = 0.015625$ d, the procedure converged for rainfall $R = 0.239$ m d^{-1}and $R = 0.241$ m d^{-1}, but not for $R = 0.240$ m d^{-1}. A previously successful case for $R = 0.23$ m d^{-1} failed if either Δz or Δt was halved. In such cases we found that the iterative procedure for one time-step failed after estimated ψ approached $-\infty$ at a depth node just below the wetting front. The problem was rectified, for the cases we found, by modifying the authors' constraints on the magnitude of $\Delta\psi$ between iterations. Their constraint, limiting positive changes to estimated ψ-values over most of the negative range, was changed to a bi-directional version applied to all ψ-values, combined with absolute upper and lower limits. Thus we use $|\Delta\psi| \leq 0.8\,|\psi| + k$, and $\psi_{min} \leq \psi \leq \psi_{max}$, where k is a constant, ψ_{min} is at the negative end of a table of hydraulic properties, and ψ_{max} is computed assuming less than 1 m depth of surface ponding. None of the values of constants in this constraint are critical, using either soil model.

We found that a further modification of the numerical scheme of Ross and Bristow, to use geometric mean hydraulic conductivity instead of their arithmetic mean, increased the upper limit of Δz for numerical convergence and stability (using the Campbell soil model). With this change, equations (4.15) to (4.18) yield a complete difference scheme using:

$$q^{l}_{k+0.5} = K^{l}_{k+0.5} - \frac{U^{l}_{k+1} - U^{l}_{k}}{\Delta z_{ck}} \qquad (4.21)$$

$$K^{l}_{k+0.5} = \sqrt{K^{l}_{k}\ K^{l}_{k+1}} \qquad (4.22)$$

where k is depth i or $i+1$, and l is time j or $j+1$.

The geometric mean causes some numerical sharpening of the wetting front (*Warrick*, 1991; *Li*, 1993) with any soil model, and partially compensates for numerical diffusion caused by using a 'fully implicit' or backward difference scheme ($\alpha = 1$) when using large time-steps.

Our final change to the details of the numerical strategy of Ross and Bristow was to evaluate soil hydraulic functions using lookup tables. This increased the efficiency of computing the required soil hydraulic properties from vector [ψ], the estimate of the solution computed during the previous iteration. High-resolution tables of all functions are linked, with exponential spacing of ψ-values. Thus for each element of [ψ], a simple calculation is used instead of a search to determine position on the table, and another simple calculation determines an interpolation factor used to evaluate all other soil hydraulic properties for the precise ψ-value. Use of tables, with 300 points in the range $\psi_a \geq \psi \geq -1000$ m required about 1 more iteration per time-step, but achieved faster computation per iteration. Overall computation was slightly faster, even with the very simple functions of the Campbell soil hydraulic model.

There is necessarily a slope discontinuity for each variable at every point on a lookup table used with linear interpolation. Numerical problems associated with $\partial\theta/\partial\psi = 0$ are commonly attributed to slope discontinuities (e.g. *Ross and Bristow*, 1990). But these, *per se*, cause no difficulties for Newton–Raphson solution schemes or for the numerical procedure as a whole. Discontinuous functions, non-monotonic functions, and zero slopes, however, will all cause numerical failures.

There is no speed penalty in tabulating the slightly more complicated functions and derivatives of the BW soil model to achieve determinacy and scaling, as computational speed is independent of the forms of the hydraulic functions. Further, use of tables makes the algorithm for solving the flow equation independent of the soil model, making comparison of soil models particularly easy.

For the purposes of this work, there is no time-step control during a simulation, so that if convergence fails, the procedure stops. The only control on the solution procedure, the above mentioned $\Delta\psi$ constraint, remains unchanged for all simulations. The numerical scheme described above will be used with two temporal weightings of the spatial differential, $\alpha = 0.5$ and 1.0, to determine the parameter space for numerical convergence and stability for Crank–Nicolson and backward difference schemes, respectively.

Alternative iterative schemes for solving the finite difference equation

We recognise that our choices of various numerical features, including the Newton–Raphson iterative scheme, are by no means absolute, being based on spot checks of performance. The scheme of Ross and Bristow is undoubtedly near the fast end of the computational speed spectrum. This appears to be due largely to three factors: exact mass conservation, reduction of the consequences of indeterminacy of solutions in very dry soil due to solving (4.7), and using a Newton–Raphson scheme to permit direct solution of forms of the flow equation having mixed dependent variables. However, the numerical scheme of *Celia at al.* (1990), with a modified Picard solution scheme, also conserves mass exactly. At present there appear to be no direct performance comparisons with schemes related to that of *Ross and Bristow* (1990). We therefore consider the differences between these solution schemes.

The Picard solution scheme may be used to directly solve forms of the flow equation using a single dependent variable. Thus to solve (4.4) for $[\psi]$, terms in F_i are rearranged so that the set of equations becomes the matrix equation:

$$[A]\left[\psi^{j+1}\right] = [b] \tag{4.23}$$

where the vector $[\psi^{j+1}]$ represents potentials at the end of the current time-step, the vector $[b]$ incorporates all terms involving the beginning of the time-step, time j, and element A^i_k in matrix $[A]$ is the coefficient of ψ_k^{j+1} in row i.

The Newton–Raphson solution scheme may be used to solve directly any form of the flow equation. The matrix equation is:

$$-[F] = \left[\frac{\partial F}{\partial \psi^{j+1}}\right][\Delta\psi] \tag{4.24}$$

where $[\partial F/\partial\psi^{j+1}]$ is a tridiagonal matrix of the derivatives of (4.15) – (4.18) with respect to ψ (sometimes referred to as a Jacobian matrix), and vector $[\Delta\psi]$ yields a correction to the existing estimate of $[\psi^{j+1}]$.

The complete algorithm has nearly identical structure with either Picard or Newton–Raphson solution scheme. Firstly, matrix $[A]$ is tridiagonal, and is solved very rapidly and accurately using the Thomas algorithm (e.g. *Press et al.*, 1986). Secondly, the matrix equation is solved iteratively, each time using the previous estimate of $[\psi^{j+1}]$.

Apart from the algorithm, major differences do exist between these schemes. The conceptual difference is that the Newton–Raphson scheme applies directly to all forms of the flow equation. Further, *Paniconi et al.* (1991) showed that the Newton–Raphson scheme converged more

quickly, and over a wider Δt range, yielding slightly faster computation for infiltration into relatively dry soil. They argued that the Newton–Raphson scheme is more difficult to implement, on the grounds of greater complexity. But we found that despite having slightly more complex algebra, individual matrix and vector elements are mathematically and physically more intelligible. Because of this, and the ease of determining whether errors are in the vector or the matrix, we found that it was easier to implement the Newton–Raphson scheme.

Various workers have investigated or used modified Picard schemes (e.g. *Huyakorn et al.*, 1984; *Milly*, 1985; *Celia et al.*, 1990; *Kirkland et al.*, 1992) or modified Newton–Raphson schemes (*Cooley*, 1983; *Huyakorn et al.*, 1984; *Allen and Murphy*, 1985, 1986; *Li*, 1993). In each case, a scheme for solving (4.4) was modified to obtain indirect solutions of (4.3), which has mixed dependent variables. In each case the concept is to split a finite difference representation of the temporal derivative of (4.4) into two parts. The major part is approximated, during each iteration, by directly using $\Delta\theta/\Delta t$ from the immediately preceding iteration. The difference between these two iterations is used in the procedure for solving for $[\psi]$, the vector comprising matric potentials at all depth nodes.

Both modified schemes are significantly more complex than *Brutsaert's* (1971) direct Newton–Raphson solution of (4.3). The above-mentioned works indicate the need for very small Δt values near the start of a simulation, whereas *Brutsaert* (1971) and *Ross* (1990) used relatively large fixed time-steps. *Huyakorn et al.* (1984) found that a modified Picard scheme converged much more slowly, and over a smaller range of conditions, compared with a modified Newton–Raphson scheme. These facts suggest that modified Picard schemes, which are becoming well known, are less efficient than modified Newton–Raphson schemes, and that both are considerably less efficient than direct solution of (4.3).

Having said this, it seems that *Celia et al.* (1990) are unnecessarily conservative, claiming only that their modified Picard scheme is not slower than the traditional Picard solution of (4.4). Their explanation of matching Δt constraints seems to be applicable only to a single time-step, with matching initial conditions. By contrast, *Huyakorn et al.* (1984) found modifications were required to improve the numerical efficiency of Picard schemes.

In the absence of direct performance comparisons, we shall assume that the efficiency of the modified schemes is intermediate between that of direct solutions of (4.3) and (4.4).

4.9.7 Scaled solutions

We now present scaled numerical solutions and compare them with analytical solutions, to demonstrate the accuracy achieved by our numerical scheme with moderate to very large fixed node

spacing. The examples are for the numerically demanding problem of constant-flux infiltration into extremely dry soil, using a Crank–Nicolson finite difference scheme ($\alpha = 0.5$), unless stated otherwise.

Fig. 4.5 shows a case of constant-flux infiltration into a semi-infinite dry soil, using the ordinary dimensionless variables of the BW soil hydraulic model (*qv.* Table 4.4). The dry initial condition is represented by $\psi^* = -10\,000$, corresponding to matric potentials more negative than –1000 m for most soils. Rainfall, given by $R^* = 0.5$, is relatively high, and the dimensionless soils in Fig. 4.5 are represented by $C = 1.02$ and $C = 1.5$. The fixed node spacings are $\Delta z^* = \Delta t^* = 0.25$. Analytical solutions are shown for comparison.

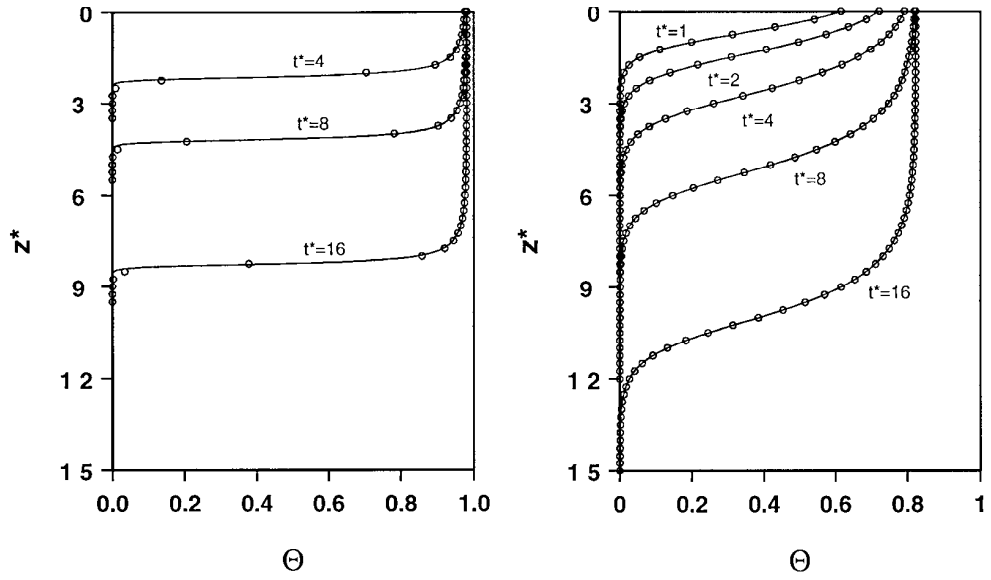

Fig. 4.5. Comparison of dimensionless numerical and analytical solutions for constant-flux infiltration, $R^* = 0.5$, into a semi-infinite 'dry' soil profile, represented by $\psi^* = -10^4$ for (a) highly nonlinear soil, $C = 1.02$, (b) weakly nonlinear soil, $C = 1.5$.

The numerical solutions of Fig. 4.5a, for the case of a highly nonlinear soil represented by $C = 1.02$, exhibit the theoretically expected 'travelling wave' (*Philip*, 1958), a wetting front of constant shape. Over most of the Θ-range, agreement between the analytical and numerical solutions is very close. Each numerical wetting front is more diffuse than the analytical solution at the leading edge ($\Theta < 0.05$). In this region the depth node spacing is too large to permit good piecewise linear representation of the moisture profile. At the end of the first time-step we found that the analytical wetting front occupied about one depth node spacing, and the numerical solution had errors in Θ of about 0.05 at the top and bottom of this range. These errors are not propagated; in fact they are greatly reduced. There is some numerical instability, manifested as spatial oscillation in near-surface Θ of the order of 10^{-4}, but it is much too small to appear on the scale the figure.

The case of a weakly nonlinear moisture characteristic (C = 1.5) in Fig. 4.b shows more diffuse wetting fronts. Here the numerical solutions correspond closely to analytical solutions throughout, even at times prior to the development of the travelling wave. We found complete freedom from numerical instability in this case. For both soils, errors in surface soil-water content Θ_0 were less than 0.1%, and far too small to appear on the figure. Mass balance errors were of the order of 1 part in 10^{12} of cumulative infiltration. With both Crank–Nicolson and backward difference schemes, we found that extreme precision is easily achieved with small node spacings.

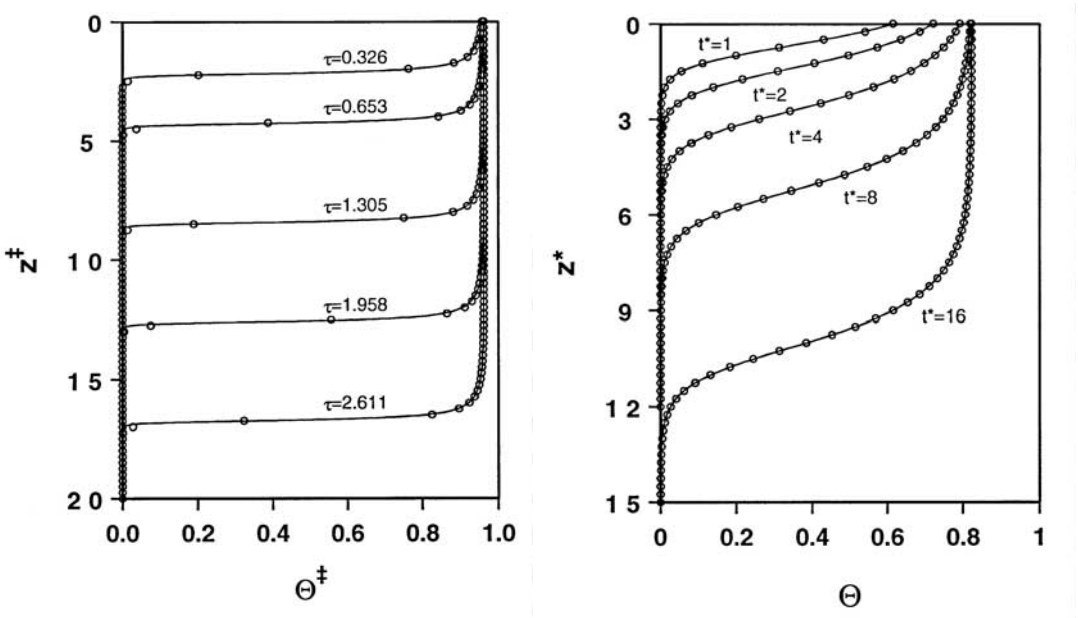

Fig. 4.6: Comparison of universally scaled (independent of soil type) numerical and analytical solutions for constant-rate infiltration into a semi-infinite 'dry' soil profile, for scaled rainfall rates (a) ρ = 6.127, and (b) ρ = 0.1667. Note that each solution scales to an infinity of cases.

Fig. 4.6 shows universally scaled solutions for constant-flux infiltration into dry soil, represented by the scaled initial condition $\psi^{\ddagger} = -10\,000$. Fig. 4.6a shows solutions for a high scaled rainfall rate ρ = 6.127. The sharp wetting fronts at scaled times τ = 0.326, 0.653, and 1.305 scale exactly to the cases of Fig. 4.5a, except for the extremely small discrepancy between the initial conditions $\psi^{\ddagger} = -10\,000$ and $\psi^* = -10\,000$. The solutions scale also to an infinity of cases with the same value of ρ, but different values of rainfall R^* and soil structure C. Physically, this says that the sharp wetting fronts shown may be due to cases ranging from that of Fig. 4.5a, with moderate rainfall into the highly nonlinear soil, to extremely high rainfall into weakly nonlinear soil. Fig. 4.6b, with the lower scaled rainfall rate given by ρ = 0.1667, likewise scales to an infinity of cases, including those for t^* = 4, 8 and 16 in Fig. 4.5b, and to very low rainfall into a highly nonlinear soil.

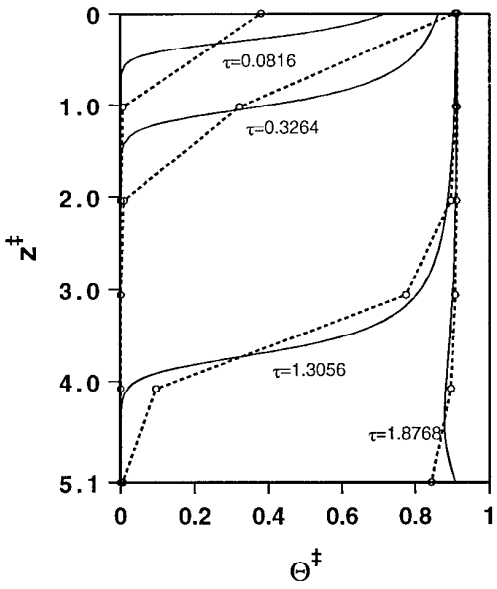

Fig. 4.7: Comparison of universally scaled numerically calculated moisture profiles with very coarse node spacings, and scaled analytical solutions for infiltration into a finite depth 'dry' soil, for ρ = 2.451. Note the lack of propagation of the severe short-time errors occurring shortly after infiltration begins.

For finite-depth soil profiles, there appear to be no numerical difficulties associated with the wetting front interacting with the lower boundary, possibly due in part to gravitational and matric potential gradients partially cancelling. Fig. 4.7 compares scaled numerical solutions, using very coarse node spacings $\Delta z^{\ddagger} = 1.0$ and $\Delta\tau = 0.0816$, with analytical solutions for a finite-depth soil profile with scaled depth $l^{\ddagger} = 5.1$, scaled rainfall rate $\rho = 2.451$, and the same extremely dry initial condition as used in Fig. 4.6. The analytical solution at the shortest time, $\tau = 0.0816$, shows that the wetting front has reached only about half way to the first subsurface depth node used for the numerical solution, which here uses a single time-step. This means that node spacings are much greater than the spatial and temporal scales of the early stages of infiltration, and numerical errors at this time are necessarily large, regardless of what numerical scheme might be used. For example, the error in computed surface soil-water content, which is only about half of the correct value, is required for trapezoidal integration of $\Theta^{\ddagger}$ (indicated by the dashed lines) to conserve mass. However, this severe short-time error does not propagate; by time $\tau = 1.3056$ some numerical self-correction has been achieved, and by time $\tau = 1.8768$ errors in $\Theta^{\ddagger}$ are relatively small.

Fig. 4.8 shows self-correction of short-time errors for another case of constant-flux infiltration into a finite-depth dry soil profile, using a backward difference scheme (α = 1.0). The initial condition is unchanged, scaled soil depth is $l^{\ddagger} = 5.85$ and rainfall is $\rho = 0.796$. In this case $\Delta z^{\ddagger} = 0.585$, which is small enough to permit accuracy in a piece-wise linear representation of an analytical solution, and $\Delta\tau = 0.1$. The Crank–Nicolson difference scheme yielded close correspon-

dence with analytical solutions at all times. Backward differencing necessarily causes some numerical diffusion, which is evident in the wetting front at time $\tau = 0.2$. Errors associated with numerical diffusion progressively self-correct with time, as the initially high spatial and temporal gradients in $\Theta^{\ddagger}$ decrease. Once the travelling wave has developed, by about time $\tau = 2$, errors in the numerical wetting front remain stable, until the front begins to interact with the lower boundary. Then gradients again decrease, and the numerical solution at time $\tau = 4.67$ is quite accurate.

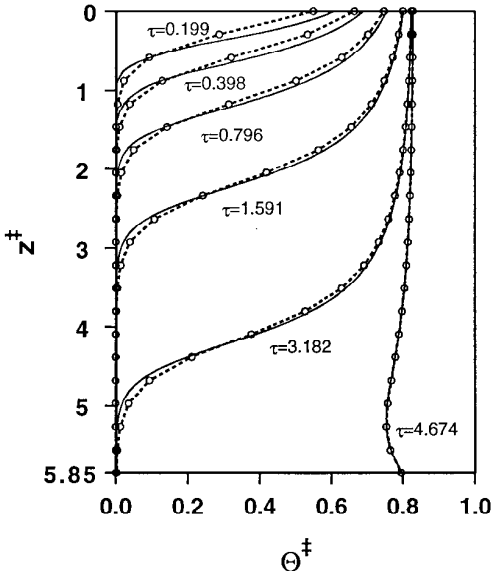

Fig. 4.8: Comparison of scaled analytical and numerical solutions for backward differencing in time, for scaled constant-flux infiltration given by $\rho = 1.05$. Note the freedom from propagation of errors, and self-correction of errors where spatial and temporal gradients decrease with time.

Numerical diffusion is determined by time-step $\Delta\tau$, as well as the gradients noted. For a linear CDE, *Noye* (1990) gives $v^2\Delta t/2$ as the numerical diffusion coefficient. For the nonlinear Richards' equation with universally scaled variables, the numerical diffusion coefficient then becomes $U^{\ddagger 2}\Delta\tau/2$; the functional form may be derived from Table 4.5.

In practice, numerical solutions for field situations will not used scaled variables. Fig. 4.9 illustrates the accurate numerical equivalence between numerical solutions obtained with and without scaling. The initial condition is $\psi^* = -10\,000$, and we have selected $C = 1.5$, $R^* = 0.2$, $l^* = 5.0$, $\Delta z^* = 1.67$ and $\Delta t^* = 4$. Solutions represented by dashed lines were obtained by transforming the initial and boundary conditions to universally scaled variables ($\rho = 0.0667$, $\psi^{\ddagger} = -10\,000$, $l^{\ddagger} = 7.5$, $\Delta z^{\ddagger} = 2.5$, $\Delta\tau = 12$), solving the flow equation with these variables, and scaling back. Here the circles represent solutions obtained without scaling. Discrepancies in Θ between scaled and unscaled solutions are less than 10^{-5} in each case. These could be reduced to computational round-

off error by scaling the initial condition and all details of the numerical procedure, for example, soil hydraulic property tables and the convergence criterion.

Using the hydraulic properties of the structured surface soil example in section 4.9.4, Fig. 4.9 could apply to a structured soil having depth 0.5 m, with a high rainfall rate R = 1.0 m d^{-1}. Exact solutions are approximated well using space step Δz = 0.167 m, and time-step Δt = 0.16 d. The spatial discretisation here is about as coarse as that used in less physically rigorous models that generalise the Green–Ampt infiltration model to multiple sharp wetting fronts as an alternative to solving Richards' equation (e.g. *Markar and Mein*, 1985). *Short et al.* (1995) demonstrated that Richards' equation based models are competitive with these, even on the basis of CPU time.

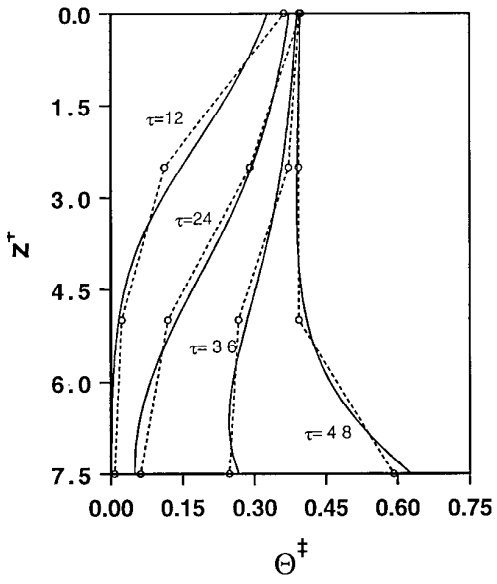

Fig. 4.9: Comparison of numerical and analytical solutions for constant-rate infiltration into a semi-infinite 'dry' soil for ρ = 0.0667, using extremely coarse node spacings. Dashed lines and symbols represent respectively numerical solutions obtained with and without solving the flow equation with scaled variables, illustrating easy attainment of accurate equivalence between scaled and unscaled solutions.

As mentioned earlier, universal scaling is not applicable to satiated conditions. However, the resulting quasi-linear CDE yields much simpler scaling and numerical performance prediction, the flow problem is highly diffusion dominated (in unconfined aquifers), and numerical solution is straightforward. Extension to 3-dimensional flows should also be easy, since horizontal flux has no convective (gravitational) component, and horizontal flows are fully diffusion dominated.

4.9.8 Criteria for guaranteed numerical convergence and stability

Numerical convergence was obtained without difficulty for all cases in section 4.9.7. With coarse discretisation, the extremely dry initial conditions required about 20 iterations per time-step, compared with 5–7 iterations for moderate discretisation and relatively moist initial conditions. No oscillation of estimated solutions was observed during the iterative process, and solutions approached their final values asymptotically. There was usually complete freedom from numeri-

cal instability, except for the very low-amplitude oscillation noted for the demanding case of Figs. 4.5a and 4.6a.

We now use scaling to search the parameter space $(\Delta z^{\ddagger}, \Delta\tau, \rho)$, in order to develop criteria for complete freedom from numerical instability and convergence failure. This is a practical alternative to searching the 4-dimensional space $(\Delta z^*, \Delta t^*, R^*, C)$ required using the BW soil hydraulic model without universal scaling, or the still higher dimensioned space required when dimensioned variables, such as in other soil models, are used.

von Neumann instability

Instability in the von Neumann sense is the propagation of perturbations as the solution proceeds in space and time (e.g. *Noye*, 1990). Linear CDEs are unconditionally stable in this sense, for both Crank–Nicolson and backward difference schemes (*Narasimhan*, 1976; *Noye*, 1990).

In this work we did not encounter this type of instability under any conditions with scaled solutions of Richards' equation. This is to be expected because the flow problem is diffusion dominated with $P_e < 2$ and $C_o < 1$ for all $\Theta^{\ddagger}$, with depth node spacing much coarser than those used in section 4.9.7. In particular, because $P_e^{\ddagger} \rightarrow 0$ as $\Theta^{\ddagger} \rightarrow 0$, numerical instability cannot be expected at the leading edge of the wetting front, as the problem is completely diffusion dominated. Diffusion dominance should assure freedom from von Neumann instability, but this does not necessarily guarantee freedom from other numerical problems.

'Wiggles'

Another numerical problem encountered with linear CDEs is the spatial oscillation that sometimes occurs at and near boundaries, but which need not propagate as the solution proceeds. This type of perturbation of the solution, described as 'wiggles' by *Roache* (1976), is caused by discretising the flow equation at the boundaries. It is most prominent with prescribed concentration boundary conditions, but occurs also with flux boundary conditions and in steady-state solutions (*Roache*, 1976), so that it cannot be eliminated over the whole parameter space using backward difference schemes.

We encountered 'wiggles' in some scaled solutions of Richards' equation, and for the purposes of this work, we include both von Neumann instability and wiggles in the term 'numerical instability'. This is because the small spatial scales of many soil-water flow problems relative to *D*- and *K*-values make 'wiggles' undesirable.

Guaranteed convergence

To guarantee obtaining solutions using the very fast Thomas algorithm for the tridiagonal solution matrix (see section 4.9.6), the matrix must be diagonally dominant. This imposes an upper limit of a little over 2 on P_e (*Noye*, 1990), and we have seen from section 4.9.4 that this imposes an upper limit on the space step of $\Delta z^{\ddagger} \cong 8$, or $\Delta z \cong 8\ \lambda_c / C$.

It should be noted that solvability of the solution matrix is necessary, but not sufficient, to guarantee that the iterative solution procedure required for a nonlinear CDE will converge. With coarse node spacings, for example, initial estimates of solutions may be inadequate for this purpose. We found convergence failures for $\Delta z^{\ddagger} = 8$, in some cases when ρ was high. The parameter space must be searched to find the region of convergence.

We searched the parameter space $(\Delta z^{\ddagger}, \Delta\tau, \rho)$ to determine the region in which solutions were both convergent and stable for constant-flux infiltration into extremely dry soil, with initial condition $\psi^{\ddagger} = -10\ 000$. The criterion for freedom from numerical instability was that any spatial or temporal oscillation in $\Theta^{\ddagger}$ should have amplitude less than 10^{-6}. The space was searched over a grid with successive values of each parameter differing by a factor of $\sqrt{2}$. This gives performance maps without smooth boundaries between numerical success and failure, but provides practical criteria for guaranteed numerical performance.

Using the Crank–Nicolson difference scheme, we found constraints on both $\Delta z^{\ddagger}$ and $\Delta\tau$, for convergence and stability for given ρ. It is practical to map the time-step limit $\Delta\tau_{max}$ as a function of ρ, for given $\Delta z^{\ddagger}$. However, we found that $\rho\,\Delta\tau_{max}$, the scaled cumulative infiltration during the time-step, shows only weak dependence on ρ. This is shown in Fig. 4.10a, for $\Delta z^{\ddagger} = 1$. Similar maps could be produced for different space steps, to show the resulting weak constraints on time-step. It can be seen that a simple practical criterion for guaranteed numerical convergence and stability with relatively large node spacing is: $\rho\Delta\tau < 0.1$, for $\Delta z^{\ddagger} \leq 1$. This criterion is quite conservative, as is shown by the examples in Figs. 4.5a and 4.6a. There $\rho\,\Delta\tau = 0.125$ and the solution just fails our stability criterion, due to wiggles in near-surface $\Theta^{\ddagger}$ having amplitude about 10^{-5}; although for most purposes stability would be regarded as very good.

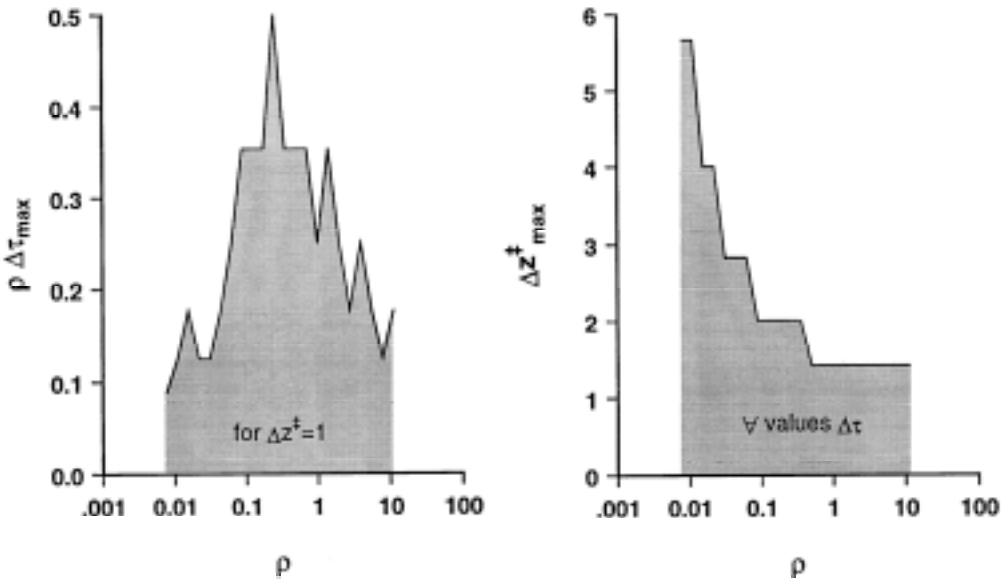

Fig. 4.10: Maps of domains of allowable step sizes which give complete freedom from numerical instability in terms of universal parameters (a) upper bound of $\rho\Delta\tau$ for the Crank–Nicolson difference scheme, (b) upper bound of $\Delta z^{\ddagger}$ for the backward difference scheme, which may be approximated by $1.4/\Theta_e^{\ddagger}$.

When a backward difference scheme (α = 1) is used, we find that numerical convergence and stability are independent of $\Delta\tau$ over an extremely wide range. This permits mapping performance in a two-dimensional plot, using the space $(\Delta z^{\ddagger}, \rho)$. Fig. 4.10b shows $\Delta z^{\ddagger}_{max}$ as a function of ρ. While this difference scheme yields a larger region for guaranteed convergence and stability, it yields slightly less accurate solutions. This can be seen, for example, in Fig. 4.8, where scaled parameters lie in the guaranteed performance space of both schemes.

We see in Fig. 4.10b that the upper bound for $\Delta z^{\ddagger}$ for numerical stability is approximately $\Delta z^{\ddagger}_{max} \leq 1.4/\Theta_e^{\ddagger}$, where $\Theta_e^{\ddagger}$ is the equilibrium surface moisture after the travelling wave is fully developed, given by $\Theta_e^{\ddagger} = 2\rho(\sqrt{1+1/\rho} - 1)$ (*Broadbridge and White*, 1988, eqn (46)). A simpler and generally conservative criterion for all soils and rainfall rates is: $\Delta z < \lambda_c$, where λ_c is the macroscopic capillary length used to scale depth and potential, as discussed in § 4.9.4. The dependence of the more precise criterion on $\Theta_e^{\ddagger}$ is consistent with our observation that numerical stability is most difficult to achieve at the surface, with a well developed travelling wave. At this point, $\Theta_0^{\ddagger}$ has its greatest value for the simulation, and wiggles are most likely to be initiated. This point cannot be explained in terms of the Péclet number, which has its maximum here only for relatively low scaled rainfall rates, *viz.* $\rho < 0.125$ ($\Theta_e^{\ddagger} < 0.5$). While a simple justification for the numerical performance criterion for higher values of ρ does not seem possible, it is tempting to speculate that a basis will be found for the convergence and stability criterion: $\Delta z^{\ddagger}_{max} \leq \sqrt{2}/\Theta_e^{\ddagger} < 8$.

Other criteria may be developed for guaranteed performance, for example, for accuracy with constant-flux infiltration, or for prescribed potential boundary conditions. Criteria for the latter case, which may be somewhat tighter, would be appropriate for modelling ponded infiltration. These are beyond the scope of this work, which is concerned with models of soil-water dynamics under natural rainfall. For such models (e.g. *Dawes and Hatton*, 1993; *Dawes and Short*, 1993), when ponding occurs during rainfall, soil is relatively moist at the beginning of the time-step, and the criterion presented here suffices. To date, we have achieved robust convergence for simulations of unsatiated/satiated soil-water dynamics for more than 100 000 soil-column years, with widely varying soil types, soil layering and weather conditions.

4.9.9 Discussion

Scaling and determinacy of solutions have been used in this work to guarantee numerical convergence and stability of solutions of the flow equation. These principles provide a technique for testing alternative numerical solution schemes more comprehensively than previously.

The ability to test numerical schemes comprehensively eliminates the need to rely on the usual *ad hoc* spot checks on numerical performance. Any choice of numerical scheme or refinements can be tested in this way. A particularly useful example would be to compare the efficiency of the modified Picard scheme of *Celia et al.* (1990) with direct methods of solving (4.3). Such testing would assist modellers to choose effectively from the plethora of available numerical schemes.

Comparisons between numerical schemes are not needed for all aspects of performance. For example, the parameter space for guaranteed convergence and stability may be examined directly. Further, accuracy may be tested by comparison with analytical solutions. However, direct comparison with an informal numerical standard is desirable, to examine computational speed comprehensively.

CPU time does not provide an ideal basis for comparison, due to rapidly changing computer technology. This situation is changing, however, with the evolution of standard measures of computer performance. Further, differences in computer architecture will have little effect on relative speeds if nearly all of the computational effort is devoted to arithmetic, which is itself a computationally efficient strategy. This may be achieved by computing hydraulic properties from $[\psi]$ during each iteration either analytically, or by using tables structured to avoiding searching, as we have done here (*qv.* section 4.9.6).

A useful alternative approach is to compare numbers of nodes and numbers of iterations required per time-step. This is because many numerical schemes have similar computational effort per iteration. In a preliminary investigation we found, for example, that for the various forms of the

flow equation discussed in section 4.9.2, with direct use of either Newton–Raphson or Picard solution schemes, and for various representations of midpoint hydraulic conductivity, computational speed per iteration did not vary by more than a factor of 2. Further, it appears from *Celia et al.* (1990) that the modified Picard scheme, in spite of additional conceptual complexity, requires very little additional computational effort per iteration.

For the algorithm reported in this work, the number of iterations per time-step varies by less than an order of magnitude over a very wide range of boundary and initial conditions, as noted in section 4.9.8. A general indication of computational speed, for the dated personal workstation used (floating point speed 1.7 MFLOPS), is 2×10^{-4} s per depth node per iteration or 10^{-3} s per depth node per time-step.

Scaling need not confine the choice of soil hydraulic model to the BW model, although there are few current alternatives. The model of *Barry et al.* (1993), for example, permits arbitrary moisture characteristics, and yields some analytical solutions. However, it appears not to permit scaling to a 3-dimensional space. It also imposes the condition $\partial^2 K^*/\partial\Theta^2 < 0$ for all Θ, so that a travelling wave solution for infiltration, which is essential for practical testing of numerical schemes, or approximating the behaviour of real soils, does not develop. One possible alternative is to recast the soil hydraulic functions and analytical solutions of the alternative approach of *Sander et al.* (1988) in terms of a practical soil hydraulic model, and to further scale to variables related to $z^{\ddagger}$, τ, and ρ. Their K and ψ functions so scaled may differ from those of *Broadbridge and White* (1988) in that K is less nonlinear, although D is common to both models.

4.9.10 Conclusions

We have shown in this work that use of the BW soil hydraulic property model provides a strategy for guaranteeing *a priori* the performance of numerical schemes for the soil-water flow equation, for prescribed flux boundary conditions. This is due to two features of the model, (a) determinacy of solutions at both the wet and dry ends of the water content range, and (b) universal scaling of solutions in terms of three parameters. The latter allows the investigation of numerical performance comprehensively over a tractable three-dimensional parameter space. This eliminates the need for *ad hoc* tests of numerical performance for each case studied, and should facilitate more general use of Richards' equation in models of soil-water dynamics.

Scaling and determinacy appear to provide powerful strategies for various purposes, including coping with numerical difficulties inherent in the non-linearity of the flow equation, and evaluating alternative numerical schemes. Preliminary work suggests that this strategy also makes numerical performance largely independent of either the choice of mass-conservative form of the

flow equation or the representation of midpoint hydraulic conductivity, using a Newton–Raphson solution scheme.

The relatively simple algorithm used here permits *a priori* choice of a coarse fixed space-time mesh, with no dynamic adjustments of the numerical procedure to deal with special cases, yet achieves high self-correction of errors that necessarily occur shortly after infiltration begins.

The allowable node spacings are so large as to suggest that they can be chosen largely on the basis of the spatial and temporal scales of the physical processes of interest. These spacings indicate the practicability of using Richards' equation as the basis for robust general purpose models of soil-water dynamics. Thus one can replace the simple two-layer models of soil-water dynamics commonly incorporated into models of crop growth (*e.g.* WAVES, *Dawes and Short* 1994, *Zhang et al.* 1996) or moisture and energy exchanges at the land surface (e.g. Shao *et al.* 1997), and even simple single-layer water balance models. Many existing models of these processes, all of which attempt to approximate solutions of equations (4.1) and (4.2), simplify solutions for numerical efficiency. However, this need not confer significant computational speed advantages over efficient use of Richards' equation (*Short et al.*, 1995), which would help to model soil-water dynamics with equivalent rigour to other parts of these models.

Acknowledgements. We thank Dr John Knight, CSIRO Centre for Environmental Mechanics, for stimulating discussions, and Dr Peter Ross, CSIRO Division of Soils, for his generosity in providing computer code for comparison with his results, and for insisting that mass balance should be exact. We thank Dr Robin Wooding of the Centre for Environmental Mechanics and Professor Wilford Gardner of the University of California at Berkeley for helpful comments. One of us, Warrick Dawes, acknowledges financial support from the Australian Water Resources Advisory Council and Land Care Australia. Another, Ian White, acknowledges support from the National Soil Conservation Program, grant 87/12 and the CSIRO Land and Water Care Program.